USING SPACEBOOK AND CESIUM TO PROMOTE AND ENHANCE FLIGHT SAFETY

Oltrogge, D.L.[1], Getz, G.[2], Vallado, D.A.[1], Alfano, S.[1], Gist, R.G.[1] , Shogren, S.[1]

[1] COMSPOC Corporation, 7150 Campus Dr. Ste 260, Colorado Springs CO 80920 USA, Email: cssi@comspoc.com
[2] Cesium, 400 Market Street, Philadelphia, PA, USA, Email: gabby@cesium.com

ABSTRACT

The paper gives an overview of the key constituents of the Spacebook portal, including: (1) a highly performant, Cesium-based space population "Explorer;" (2) space weather; (3) Earth orientation parameters; (4) a synthetic covariance information; (5) a comparative Space Situational Awareness (**SSA**) "live" analyses; (6) XP-TLEs fitted to all public objects in the SP High-Accuracy Catalog; (7) a technical library of COMSPOC-authored content; (8) a technical video library; (9) a Rendezvous and Proximity Operations (RPO) analysis section; (10) reference orbits and comparisons with a variety of SSA positional knowledge products; (11) a download portal with APIs to obtain and interact with content; and (12) a space standards informational tab and with reference links.

1 Introduction

1.1 Using Spacebook and Cesium to promote and enhance flight safety

A central tenet of space safety and sustainability is that of data portals and employment of data exchange using standardized data formats and exchange mechanisms. The new Spacebook portal, https://spacebook.com/, is an internet-based service designed to provide global access to essential SSA and Space Domain Awareness (**SDA**) data that spacecraft owners, operators, SSA centres, and academia need to inform their operations, activities, and analyses.

SGP4-XP represents a new propagator available to the public through the United States Space Force (USSF) dynamic link library (.DLL) on the Space-Track.org website. SGP4-XP is a new semi analytical theory that replaces the previous SGP4 theory with more realistic force models in all orbital regimes, especially above LEO. The new theory also accommodates the ballistic coefficient for atmospheric drag and the solar radiation pressure coefficient. These new coefficients occupy the TLE fields formerly used by SGP's Bstar and mean motion double dot, respectively.

Because SGP4-XP is a semianalytical model that incorporates refined perturbation models, positional accuracy can be significantly more accurate (i.e., a five or ten-fold improvement) than the older SGP4 TLEs. But note that these new SGP4-XP TLEs are only compatible with the USSF SGP4-XP DLL library.

Spacebook converts ephemerides (obtained from any source) to SGP4-XP TLEs via a simple differential correction scheme. Users having the USSF SGP4-XP software DLL library may find these SGP4-XP TLEs useful for routine operations and analyses.

The technical videos card links to COMSPOC's website, to a page that contains videos produced by COMSPOC's research and operations teams. These videos show recent events that have happened in space, modelling and predictions of potential threats, as well as the results of research studies.

The Spacebook Explorer is a Cesium-based 3D visualization engine with which you can see what is currently happening in space. The default explorer window shows all space objects in the current Spacebook catalog. Each dot represents a space object and is coloured according to the following default scheme: (a) Active satellites – green; (b) Rocket bodies – red; (c) Inactive satellites – yellow; (d) Debris – grey; and (e) Unknown – white.

The core functionality of Spacebook is the ability to download space data to use in your own missions or applications. There are two ways to download data: through the user interface or through the API. Users can run bulk downloads for TLE, space weather, EOP, and satellite catalog files. To download a bulk set of data, click one of the options on the right side of the window in that row. Synthetic covariance and XP-TLEs for any public space object can also be downloaded, even for a filtered list of satellites. Some objects also have reference ephemeris, which you can download if the download icon is shown under the reference ephemeris column for that object.

Proc. 9th European Conference on Space Debris, Bonn, Germany, 1–4 April 2025, published by the ESA Space Debris Office
Editors: S. Lemmens, T. Flohrer & F. Schmitz, (http://conference.sdo.esoc.esa.int, April 2025)

1.2 What is Spacebook?

Spacebook (**Fig. 1**) is an internet-based service that has a goal of providing users access to the space situational awareness (SSA) data they need, whatever their mission.

2 Spacebook components

Fig. *2*, excerpted and updated from [1], portrays the entangled relationships between force models and space object information and orbit propagation (highlighted in yellow), orbit determination and the data that feeds it (highlighted in green), dataflows and ops tempos (highlighted in orange), and the downstream analytics processes that depend upon it (highlighted in purple). Generally, SSA and SDA requirements are placed upon the accuracy, transparency, timeliness, and completeness of the downstream analytics, but those requirements in turn place demanding derived requirements upon all of the upstream components which feed it. This fact is often not recognized or acknowledged.

One of the primary goals of Spacebook (freely accessible at https://spacebook.com/) is to address these derived requirements and facilitate the operation of globally better SSA and SDA systems. The current and near-future elements of Spacebook are shown in **Fig. 3**. These elements address many of the components of SSA and SDA systems as shown in **Fig.** *4*. Among the most significant of these elements, typically responsible for some of the most egregious SSA errors, are (1) atmospheric drag, and (2) maneuvers.

For low-LEO orbits, drag modelling and prediction are particularly difficult. The principal challenges are (a) atmospheric drag models of sufficient granularity and fidelity to properly account for localized neutral density and its time dynamics; and (b) forecasting of solar and geomagnetic indices and proxies required by such an atmosphere model.

The "maneuver" category encompasses much more than simply knowing that a maneuver did or will take place; one must also be able to (a) accurately calibrate the spacecraft's maneuvers, thruster performance, and pointing errors; (b) accurately model the effects of planned maneuvers; (c) fit accurate trajectories through past maneuvers; (d) accurately predict (or propagate) trajectories through future maneuvers; and (e) accurately assess and incorporate maneuver uncertainties into the downstream positional and velocity uncertainties to assess their effects on SSA information and the Space Domain Awareness (SDA) upon which it is based.

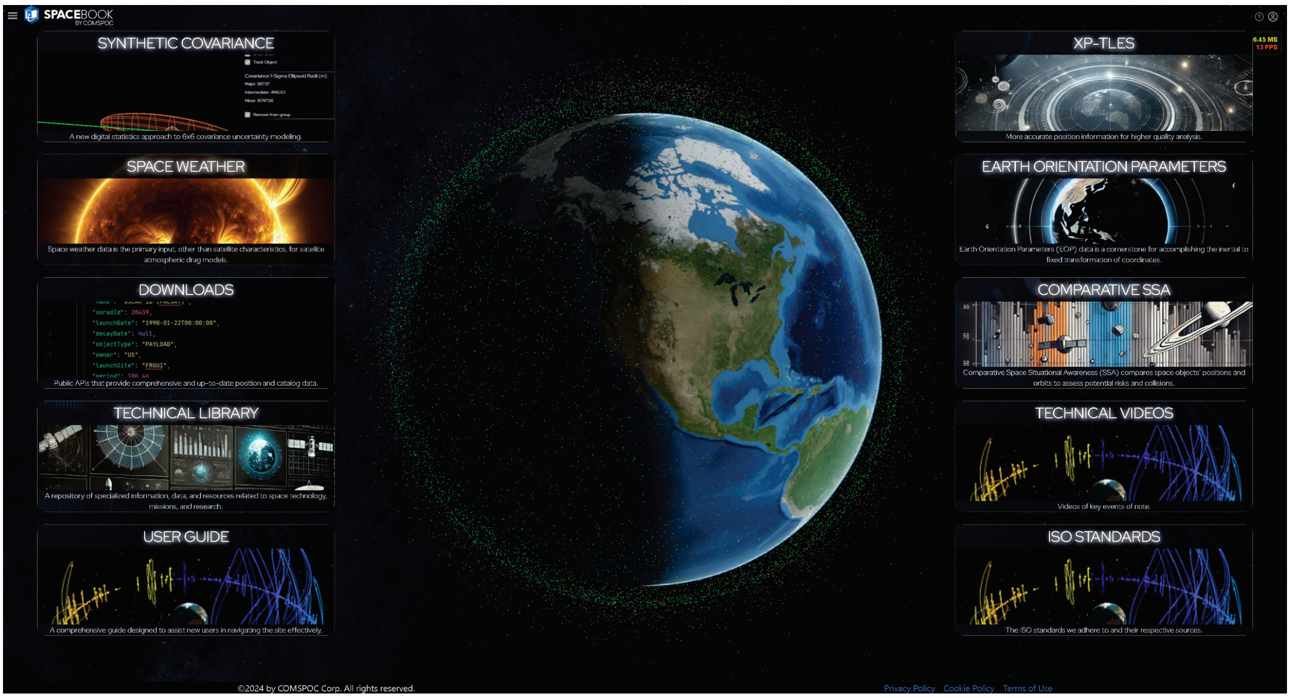

Fig. 1 – ***Spacebook homepage.***

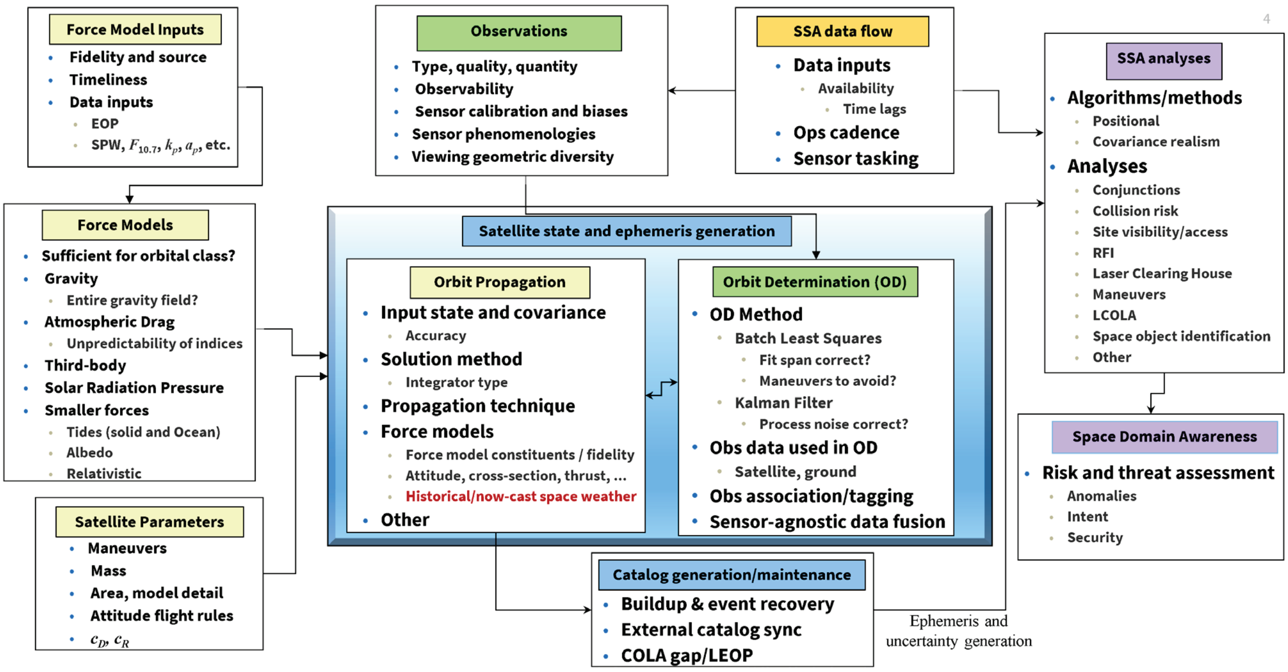

Fig. 2 – *Interrelationship between factors affecting SSA and derived SSA products.* *The satellites' orbital state generation and prediction is central to SSA and SDA. Many of the factors shown here are entangled, making optimization of SSA and SDA processes difficult in isolation.*

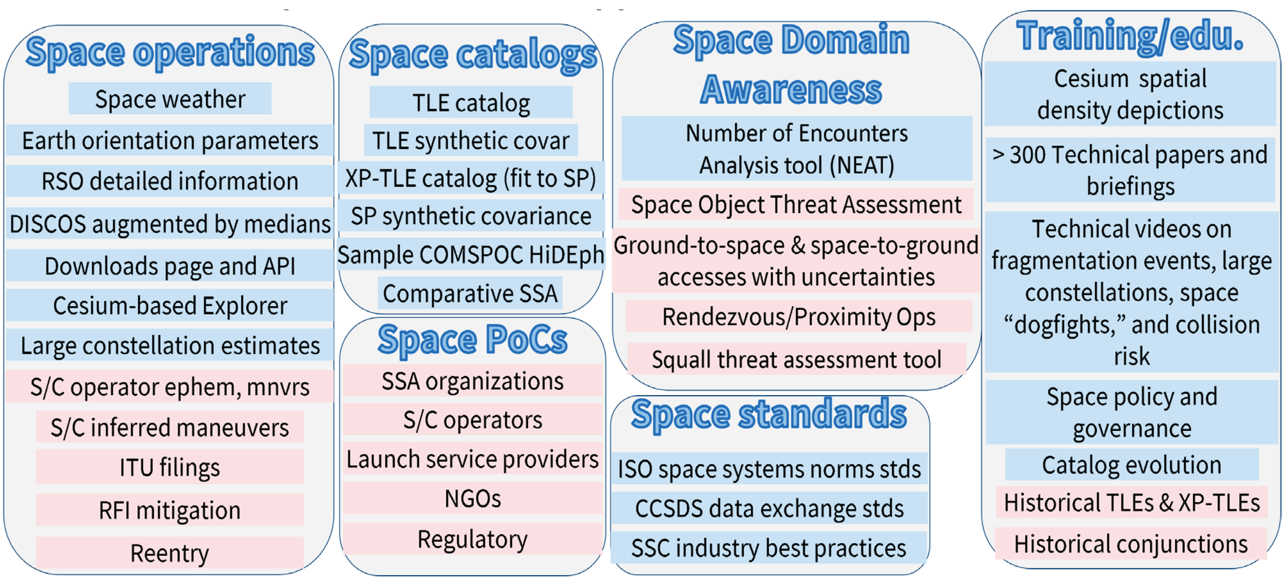

Fig. 3 – *Main Spacebook.com elements, with blue topics populated, and pink denoting near future additions.*

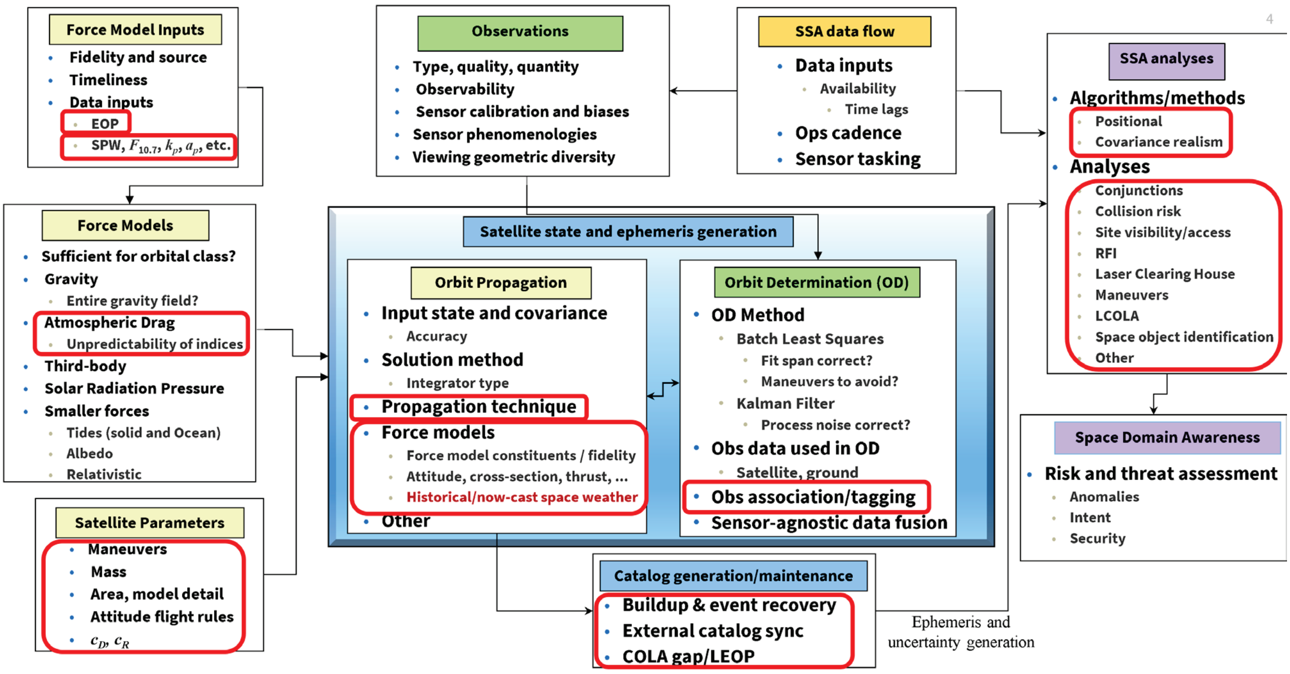

Fig. 4 – *Interrelationship between factors affecting SSA and derived SSA products.* *The satellites' orbital state generation and prediction is central to SSA and SDA. Many of the factors shown here are entangled, making optimization of the process difficult in isolation.*

3 Earth Orientation Parameters

Having consistent Earth Orientation Parameters (EOP) and reference frame definitions [3] is a cornerstone for ensuring consistent reference frame transformations between multiple spacecraft operators and/or SSA centres. Most numerical propagators integrate in an inertial frame, while observations and force model accelerations are applied in a fixed reference frame. The Spacebook aggregates historical final values together with short-, medium-, and long-term EOP predictions to help space organizations standardize such transformations.

The EOP information consists of ΔUT1, the difference between UT1 (Universal time) and UTC (Coordinated Universal time), the length of day, polar motion coefficients (x_p, y_p) describing the movement of the Earth's rotation axis to the crust. Nutation parameters for the older IAU-76/FK5 theory ($\delta\Delta\psi$, $\delta\Delta\varepsilon$) and the coordinate parameters (dX, dY) for the IAU-2010 conventions are also included. The number of leap seconds between UTC and TAI (Atomic time), ΔAT, is not generally considered an EOP parameter *per se*, but we include it as it is necessary to implement inertial to fixed transformations, and it is valuable to have all the parameters in a single file. The EOPP files from NGA were a historical approximate form but appear not to be used anymore.

There are several files necessary to piece together a complete EOP data file that satisfies all aspects of satellite analysis. There are typically small differences between sources of EOP data (e.g., International Earth Rotation Service (IERS), and the US Naval Observatory - USNO), but the impact on overall satellite positional accuracy is usually small (a few meters or less). The USNO distinguishes two sets of values: Bulletin A that are the rapid values to about the current date, and the Bulletin B values that are the final values to within about 1.5 months of current date. **Fig. 5** and the subsequent bulleted list show the sources, parameters, and frequency of Spacebook's EOP information.

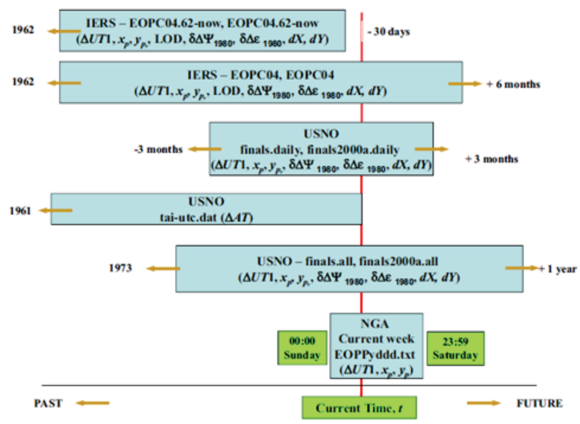

Fig. 5 – *Sources, parameters, and frequency of EOP data* *[Figure from Vallado [2] by permission].*

The following EOP sources are utilized to assemble Spacebook's integrated set of historical values and predictions:

- IERS Data
  - https://hpiers.obspm.fr/iers/eop/eopc04/ (data to the current date for both IAU-76/FK5 and IAU2006)
  - https://hpiers.obspm.fr/iers/series/opa/eopc04.txt (data to the current date and predictions for IAU-76/FK5)
  - https://hpiers.obspm.fr/iers/series/opa/eopc04_IAU2000.txt (data to the current date and predictions for IAU2006)
  - Contains: Observed data (x, y, UT1-UTC, LOD, $\delta\Delta\psi$, $\delta\Delta\varepsilon$), (δX, δY)
  - Updated: Daily
- USNO Data (we use these primarily as backup in case the IERS site is down):
  - https://maia.usno.navy.mil/ser7/finals.daily
  - https://maia.usno.navy.mil/ser7/finals2000A.daily
  - https://maia.usno.navy.mil/ser7/finals.all
  - https://maia.usno.navy.mil/ser7/finals2000A.all
  - https://maia.usno.navy.mil/ser7/finals.data
  - https://maia.usno.navy.mil/ser7/finals.datafinals.data.txt
  - https://maia.usno.navy.mil/ser7/finals2000A.data
- Leap Second Data
  - https://maia.usno.navy.mil/ser7/tai-utc.dat
  - Contains: TAI-UTC data
  - Updated: With new leap second information from Bulletin C 61 at the Observatoire de Paris

To get the latest EOP information from Spacebook, click the "recent" or "full" button under the "Download EOP Data" header on the right side of the EOP page. The "recent" button will download the last five years of EOP data while the "full" button will download EOP data dating back to 1962. You can also access these downloads through the API by pointing to: https://spacebook.comspoc.com/api/eop/full or https://spacebook.comspoc.com/api/eop/recent.

The format of the EOP file is provided in

Table 1.

4 Space weather

Space weather data is the primary input, other than satellite characteristics, for satellite atmospheric drag models. Even the smallest changes in space weather data can have large effects during propagation. The main data indices used by atmospheric models are the geomagnetic indices (a_p, K_p), and the solar flux ($F_{10.7}$). For operations, future predictions are important. For routine Orbit Determination activities, the past several weeks to months are required with some future values. Historical studies may require data back to beginning of the Space Age in 1957. We provide additional information in the file consistent with combination efforts in the past [3].

Indices such as Sunspot numbers can differ dramatically based on the source. Because these indices are generally used for B-field measurements of the Sun and not atmospheric drag calculations, we simply use the NOAA SPWC source. Comparisons to other files may differ here.

Space weather data are available through the National Geophysical Data Center (NGDC) in the National Oceanic and Atmospheric Administration (NOAA). There are several files necessary to piece together a complete data file that satisfies all aspects of satellite analysis. Because 3-hourly data are available for the geomagnetic indices, maintaining a truly current file requires frequent retrieval (at 3 hours) and assembly of the data. Note that the K_p values are all multiplied by 10. Some data fields have changed from integer to double.

Space weather data is accumulated from a variety of sources [3]. **Fig. 6** and the subsequent bulleted list show the sources, parameters, and frequency of Spacebook's space weather information.

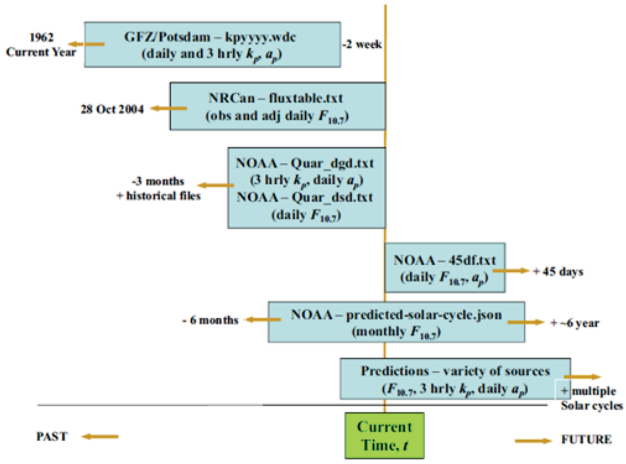

Fig. 6 – ***Sources, parameters, and frequency of space weather data*** *[Figure from Vallado [4] by permission].*

- Combined Geomagnetic and Solar Flux Data to 2017
  - ftp://ftp.ngdc.noaa.gov/STP/GEOMAGNETIC_DATA/INDICES/KP_AP/yyyy (*BSRN*, *ND*, 3-hourly K_p, 3-hourly A_p, C_p, C_9, *ISN*, $F10.7_{Adj}$, *Q*)
  - Updated: Monthly (a little over one month after end of the month)
  - Contains: Each month a *yyyy* file is produced, where *yyyy* is the year. A monthly indicator is no longer used. The NGDC files go only to about the most recent month.
- Combined Geomagnetic and Solar Flux Data 2018 to date
  - ftp://ftp.gfz-potsdam.de/pub/home/obs/kp-ap/wdc/yearly/kpyyyy.wdc (*BSRN*, *ND*, 3-hourly K_p, 3-hourly A_p, C_p, C_9, *ISN*)
  - Updated: Monthly (a little over one month after end of the month)

- Contains: This site has newer data, but does not include the solar flux values. The data goes to the end of the month, or the middle of the month depending on the update.

- Observed and Adjusted Solar Flux
  - ftp.seismo.nrcan.gc.ca/spaceweather/solar_flux/daily_flux_values/fluxtable.txt ($F10.7_{Obs}$ from 1947 Jan 01 until end of previous month)
  - Updated: Monthly (end of month)
  - Contains: These files have all the observed and adjusted solar flux values.
- Geomagnetic data
  - ftp://ftp.swpc.noaa.gov/pub/indices/quar_DGD.txt and ftp://ftp.swpc.noaa.gov/pub/indices/old_indices/yyyyQn_DGD.txt
  - (3-hourly K_p for the current quarter to date (previous quarters also available))
  - Updated: Every 3 hours starting at 0030 UT.
  - Contains: All the data from a quarter. It becomes 1 line long at the start of a new quarter, requiring the previous quarter to be held as well. n = 1-4.
- Quarterly Solar Flux data
  - ftp://ftp.swpc.noaa.gov/pub/indices/quar_DSD.txt and ftp://ftp.swpc.noaa.gov/pub/indices/old_indices/yyyyQn_DSD.txt
  - (Daily $F10.7_{Adj}$, *ISN* for the current quarter to date (previous quarters also available))
  - Updated: Daily at 0225UT, 0825UT, 1425UT, & 2025UT.
  - Contains: A ll the data from a quarter. It becomes 1 line long at the start of a new quarter, requiring the previous quarter to be held as well. n = 1-4.
- 3 Day Predictions
  - https://services.swpc.noaa.gov/text/3-day-solar-geomag-predictions.txt
  - (Current-day actuals of daily A_p and $F10.7_{Adj}$)
  - Updated: Daily at 2200 UTC.
  - Contains: This file has the previous 3 days. It is used to fill in data that may be missing from the other sources.
- 45 Day Predictions
  - ftp://ftp.swpc.noaa.gov/pub/forecasts/45DF/mmdd45DF.txt
  - (45-day forecast of daily A_p and $F10.7_{Adj}$)
  - Updated: Daily at 2114 UTC.
  - Contains: The 45-day predictions are used to fill in the daily geomagnetic and solar flux predicted values 45 days into the future.
- Monthly Predictions
  - https://services.swpc.noaa.gov/json/solar-cycle/predicted-solar-cycle.json and https://testbed.spaceweather.gov/sites/default/files/2023-10/predicted-solar-cycle_0.json
  - (Monthly *ISN* and $F10.7_{Adj}$ for approximately two years)
  - Updated: Monthly.
  - Contains: The rest of the solar cycle of predicted data, but no geomagnetic data.

4.1.1 Spacebook characterization of space weather indices and forecasts

Space weather indices and their prediction can vary widely as shown in **Fig. 7**. Spacebook maintains several standardized "live" characterizations of such fluctuations and deviations as shown in **Fig. 9**, **Fig. 10**, and **Fig. 11**.

Table 1 – ***Earth orientation parameter file format***

EOP data is provided in space-delimited format with the following fields:

```
# FORMAT(I4,I3,I3,I6,2F10.6,2F11.7,4F10.6,I4)
# ----------------------------------------------------------------------------------------------------
#   Date     MJD       x          y        UT1-UTC       LOD        dPsi     dEpsilon      dX         dY      DAT
# (0h UTC)             "          "           s           s           "          "          "          "       s
# ----------------------------------------------------------------------------------------------------
# y4 mm dd nnnnn +n.nnnnnn +n.nnnnnn +n.nnnnnnn +n.nnnnnnn +n.nnnnnn +n.nnnnnn +n.nnnnnn +n.nnnnnn nnn
# ----------------------------------------------------------------------------------------------------
#
NUM_OBSERVED_POINTS 2170
BEGIN OBSERVED
2018 01 01 58119  0.059258  0.247585  0.2163567  0.0008094 -0.105054 -0.008256  0.000118 -0.000175  37
```

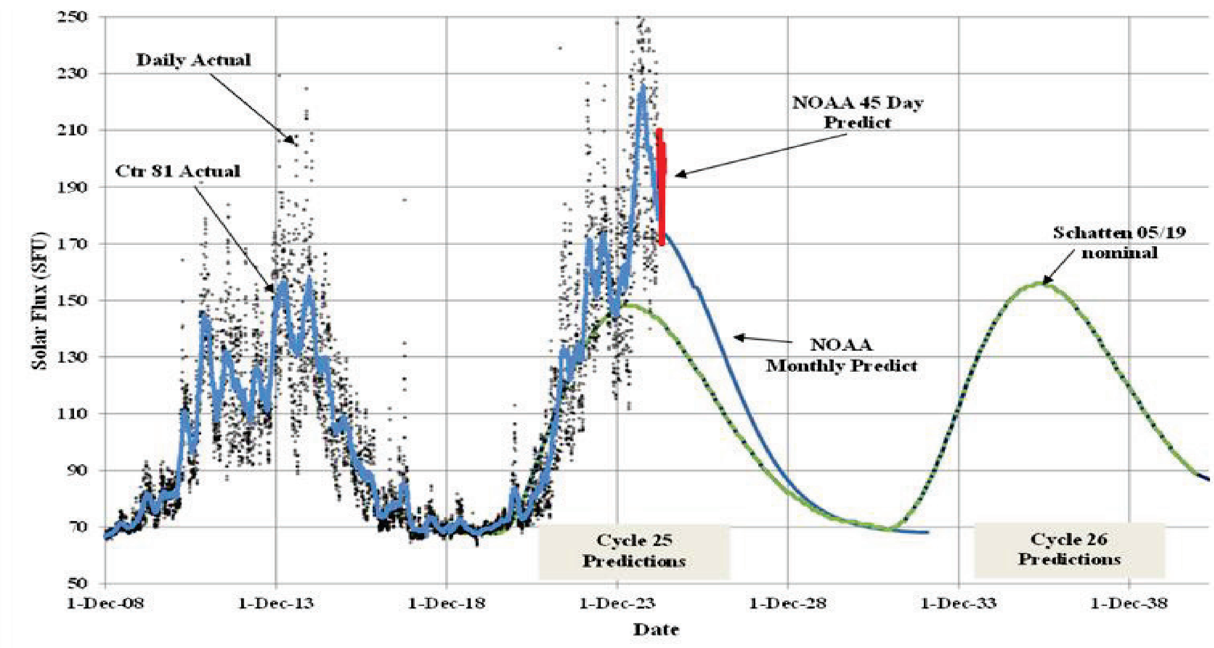

Fig. 7 – *Observed coupled with a variety of forecasted solar flux predictions.*

Table 2 – ***Space weather file format***

Space weather data is provided in space-delimited format with the following fields:

```
# FORMAT(I4,I3,I3,I5,I3,8I3,I4,8I4,I4,F4.1,I2,I4,F6.1,I2,5F6.1)
# -------------------------------------------------------------------------------------------------------------
#                                                                                          Adj     Adj   Adj   Obs   Obs   Obs
# yy mm dd BSRN ND Kp Kp Kp Kp Kp Kp Kp Kp Sum Ap  Ap  Ap  Ap  Ap  Ap  Ap  Ap  Avg Cp C9 ISN F10.7 Q Ctr81 Lst81 F10.7 Ctr81 Lst81
# -------------------------------------------------------------------------------------------------------------
#
NUM_OBSERVED_POINTS 2169
BEGIN OBSERVED
2018 01 01 2515 21 33 37 23 23 27 10 10 13 177  18  22   9   9  12   4   4   5  10 0.6 3   0  66.8 0   69.3  70.8  69.1  71.4  72.5
```

4.1.2 Space weather information

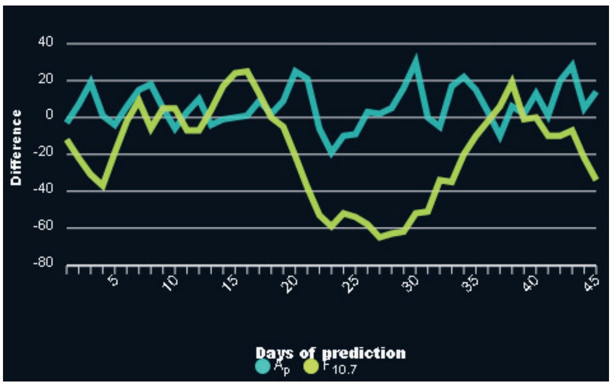

Fig. 8 – *Running characterization of Ap and F$_{10.7}$ forecast accuracy:* *View up-to-date comparisons of actual versus predicted values extending up to 45 days in arears.*

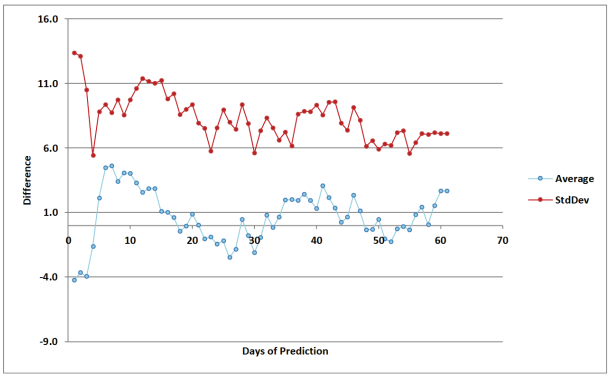

Fig. 9 – *Average and standard deviation of Ap values.*

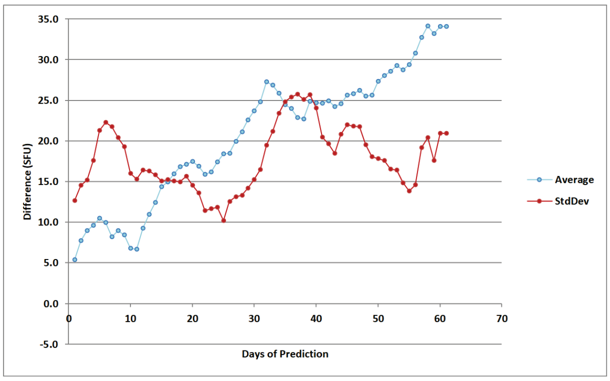

Fig. 10 – ***Average and standard deviation of $F_{10.7}$ values.***

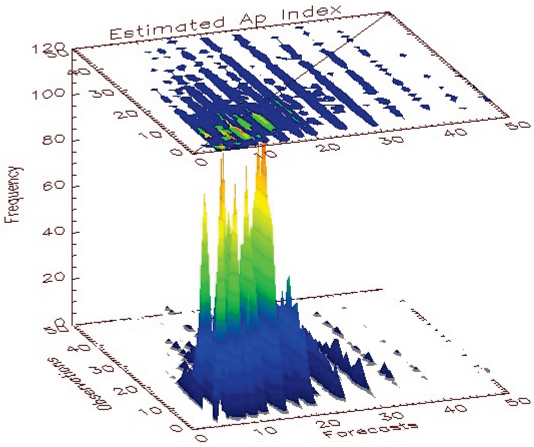

Fig. 11 – ***PDF of predicted Ap by forecast.***

The May 2024 Gannon space weather storm (**Fig. 12**) severely degraded SSA, causing more than 5,000 spacecraft to maneuver to recover their mission altitudes, phasing, and to avoid collisions, and a two-week lag in finalizing erroneous predictions of solar and geomagnetic indices led to large errors in spacecraft positional information, rendering pre-storm (and even during-storm) flight safety assessments nearly useless. The event clearly highlighted the crucial role that (1) drag plays in the LEO environment from SSA and SDA perspectives; (2) our atmospheric models need improvement; (3) our ability to accurately predict future space weather is limited; and (4) our ability to quickly react to errors in such predictions can severely limit the ability to safely operate in space for several weeks after a major storm.

For these reasons, Spacebook is designed to facilitate the rapid information of space weather information as it becomes available.

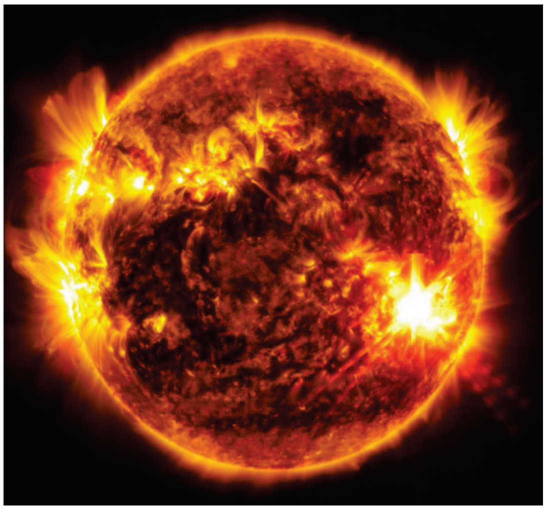

Fig. 12 – ***Gannon Storm:*** *Image from NASA's Solar Dynamics Observatory (SDO) of the Sun captured on 10 May 2024.*

5 RSO detailed information

The Spacebook draws upon and integrates Resident Space Object (RSO) data from multiple authoritative sources into a unified representation as shown in **Fig. 13**. The data primarily comes from four sources: **DISCOS** [5], **GCAT** [6], **Space-Track** [7], and **CelesTrak** [8].

Fig. 13 – ***Unified representation of aggregated RSO information.***

Fig. 14 – ***Expanded detail on RSO of interest, including notifications on upper right of multiple disparate values.***

While these catalogs often contain consistent overlapping information, they occasionally present **conflicting data**

points. When conflicts occur, Spacebook provides a visual indicator adjacent to the affected value as shown in **Fig. 15**, allowing users to identify discrepancies. Additionally, a **data quality hierarchy** is used that prioritizes sources in descending order: DISCOS, GCAT, Space-Track, and CelesTrak. This prioritization ensures that users access the highest quality available data for each value within a consolidated interface on the UI.

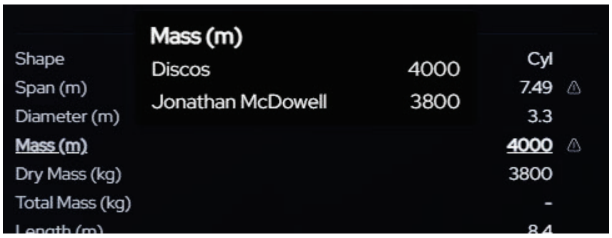

Fig. 15 – *Spacebook portrayal of conflicting data points:* *Accommodation of multiple "mass" values, by source.*

6 Synthetic covariance

Synthetic covariances are described next, accompanied by their use cases. Positional covariances are required to do an assessment of collision probability, yet often such covariances are either not available or not typically provided. Synthetic covariances offer a workaround for such cases. Spacebook provides a new digital statistics approach to 6x6 covariance uncertainty modelling that eliminates the need to assume a priori time-varying error functions for all error components and their correlations, with statistics drawn from within time and argument-of-latitude bins on an object-by-object basis. Downloads of synthetic covariances on Spacebook take the form of full ephemeris files containing 6x6 covariance information and Plotly characterizations of synthetic covariance sigmas for all objects in the public space catalog.

6.1 Ephemeris data sources for synthetic covariance generation

Due to its general nature, the synthetic covariance algorithm can be applied to any sequence of orbit predictions. It was first applied to standard two-line element sets (TLEs) propagated using SGP4 to generate ephemerides on which to perform a statistical accumulation of calculated differences. This had the benefit of being able to propagate forward and backward to eliminate any data gaps. Next, the technique was applied to "Special Perturbations" (SP) numerically integrated ephemerides obtained from Space-Track.org. And finally, the technique has now been successfully applied to Owner/Operator (O/O) ephemerides within the Space Data Center (SDC).

6.1.1 Synthetic covariance algorithm

The COMSPOC synthetic covariance assessment method uses ordered sequences of predictive positional data of variable accuracies to build up error statistics. The data is specific to partitioned by each individual RSO so as to capture actual, observed behaviours, including specific environmental or regular maneuver characteristics that may actually not show up in a normal OD process. If such characteristics change as the object's conditions change, Spacebook's method will adapt to those conditions over time. Another benefit is that curve fitting is not used; rather, the inherent dynamics of each object's orbits are contained within the data statistics, including both position and velocity components. This makes covariance estimation more accurate, especially for objects for which the full 6x6 uncertainties are not otherwise available.

It is a basic assumption of this study that when orbit tracks from different initial conditions are propagated to the same times and locations, the differences between the two tracks will primarily consist of process noise and are therefore uncorrelated. The differences are therefore expected to be normally distributed.

To prepare for the generation of synthetic covariances, the TLE, SP, and O/O catalogs are downloaded and processed daily for the past "N" weeks, where the value of N is set by the system operator. Empirical tests have shown that for many space objects, a range of 3 to 7 is ideal for the "N" value. Stepping through time from a selected beginning date, each catalog download is scanned to identify every satellite it contains.

As shown in **Fig. 16**, an ephemeris is generated (or processed) for each such satellite for a defined propagation duration, typically chosen to be 7 days. This choice of duration is consistent with propagation accuracies remaining within 1 km of the true position for a period of 1.2 to 9.2 days [9] for this type of data. The satellite's ephemeris nearest the orbit determination (OD) epoch is designated to be the current 'truth' or "reference trajectory" and is time-dependent, spanning from its orbit determination (OD) epoch until the next OD epoch for which data is obtained.

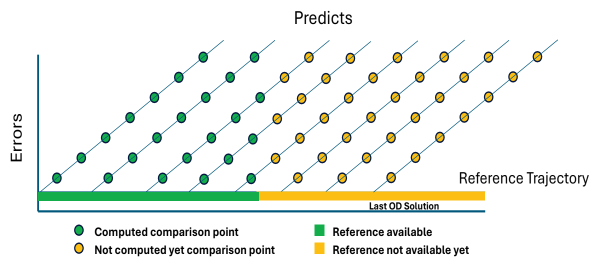

Fig. 16 – *Basic process used for overlap test statistics.*

A more detailed depiction is shown in **Fig. *17***. Illustrated is a seven-day two-line element (TLE) propagation length per update and daily updates of TLEs. The most recent ephemeris (dark line) is considered 'truth' and is differenced with previous propagations where they overlap with the 'truth'. In this illustrated case, the one day in dark highlight has overlaps with the six previous ephemerides. The difference statistics are then accumulated in time bins of a selected size. The sequence of arrows from this dark line to other overlapping predict lines illustrates the substantial quantity of differenced statistics that the technique generates.

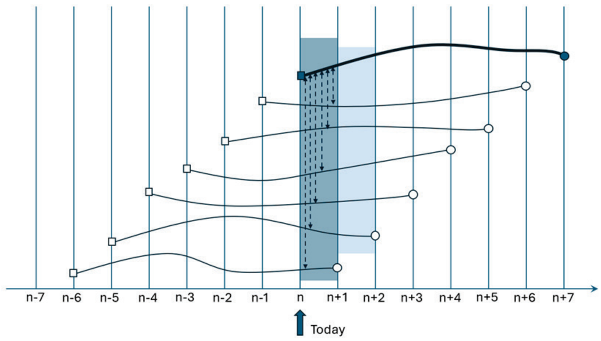

Fig. 17 – *Schematic diagram of ephemeris differences during overlap intervals.*

6.2 Selected binning approach

Testing revealed strong statistical dependencies upon both time from OD epoch and (to a lesser degree) argument of latitude. Accordingly, CSSI developed a grid binning system consisting of time bins and argument of latitude bins, as illustrated in **Fig. *18***.

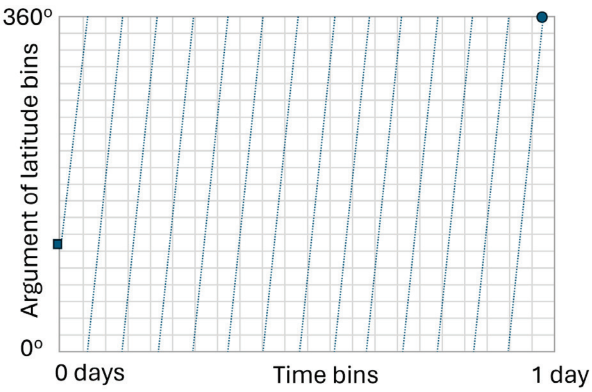

Fig. 18 – *COMSPOC synthetic covariance binning:* *Illustration of how the time bins and argument of latitude bins will get filled by difference calculations at each propagation step as the satellite orbits over a day. For a satellite at GEO, the illustrated track would span only once from bottom-left to top-right. Epoch is indicated by a square icon, and the final ephemeris time point is indicated by a circle icon.*

While one would be tempted to select very small ("granular") bins for this work, the operational synthetic covariance system reflects a careful balancing of two goals: (1) to be adaptive to long-term changes in an orbiting object's conditions (orbital environment, orbit transfer, station-keeping maneuver frequency, etc.), and (2) to be judicious in storage and processing resources, as the system would need to maintain statistics on as many space objects as possible within reasonable time and space constraints on an operational computer.

It is not useful to retain difference data from extremely old epochs for storage space considerations, so to accomplish the latter of the two goals, the memory mapping onto the hard drive storage for the statistical data per satellite corresponds to 1-week "memory cells" (termed 'eras', which could be weighted individually) with a fading memory weighting scheme. This conserves hard drive storage space and provides adaptability to major orbit change operations, for example.

The weighting for the data in the era containing the current epoch for our predictive ephemeris should have a relatively lower weighting to protect against potential data sparseness from a shortage of recent element sets. Similarly, the farthest era from the current epoch can be somewhat de-weighted, in this case to move away from older, possibly less relevant difference statistics to adapt to the object's latest conditions. The other two eras can have higher weightings, reflecting their improved data density and temporally relevant statistics. Weighting factors can be specified by the user and are notionally shown in **Fig. *19***.

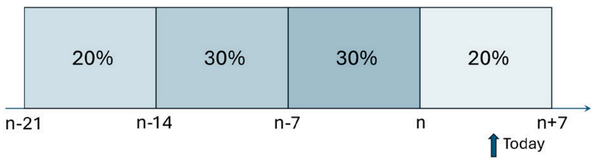

Fig. 19 – *COMSPOC time bin weighting strategy:* *A sample 4-era data weighting scheme, which is configurable by the user, is illustrated here. The newest data is down weighted because it may be the most sparse and subject to data instability. Weighting is greatest on prior data closest to the current date, and the weight decreases as the data ages. This weighting scheme is only applied during covariance reconstruction to accompany the latest 'truth' ephemeris.*

As described in [10], we calculate the variances and covariances for the six degrees of freedom in the orbit relative position $N\ T\ W$ frame, where velocity differences are denoted by $\dot{N}$, $\dot{T}$ and $\dot{W}$, and then we form the 1-sigma 6x6 covariance matrix as shown:

$$
cov_{6x6} = \begin{bmatrix} var_{NN} & cov_{NT} & cov_{NW} & cov_{N\dot{N}} & cov_{N\dot{T}} & cov_{N\dot{W}} \\ cov_{NT} & var_{TT} & cov_{TW} & cov_{T\dot{N}} & cov_{T\dot{T}} & cov_{T\dot{W}} \\ cov_{NW} & cov_{TW} & var_{WW} & cov_{W\dot{N}} & cov_{W\dot{T}} & cov_{W\dot{W}} \\ cov_{N\dot{N}} & cov_{T\dot{N}} & cov_{W\dot{N}} & var_{\dot{N}\dot{N}} & cov_{\dot{T}\dot{N}} & cov_{\dot{N}\dot{W}} \\ cov_{N\dot{T}} & cov_{T\dot{T}} & cov_{W\dot{T}} & cov_{\dot{T}\dot{N}} & var_{\dot{T}\dot{T}} & cov_{\dot{T}\dot{W}} \\ cov_{N\dot{W}} & cov_{T\dot{W}} & cov_{W\dot{W}} & cov_{\dot{N}\dot{W}} & cov_{\dot{T}\dot{W}} & var_{\dot{W}\dot{W}} \end{bmatrix} \tag{1}
$$

To populate as many cells as possible, bin sizes were kept from getting too small. Unpopulated cells cause noise in produced covariance data, which can wreak havoc in downstream estimates of collision risk.

6.3 Bilinear interpolation

As another layer of protection against spurious noise and unpopulated bins degrading covariance estimates, we introduced bilinear interpolation of covariances to improve smoothness and maximize available data density. Whenever a covariance is needed at a time, t, and argument of latitude, u, a bilinear interpolation [11] is computed from the two bounding time bins and the two-bounding argument of latitude bins.

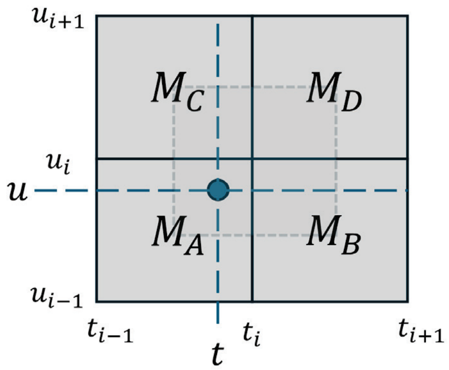

Fig. 20 – *Statistical accumulations of difference moments M:* *Portrayed in time bins (horizontal) and argument of latitude bins (vertical). M-values could represent any relevant 1st or 2nd moment used for mean, variance, or covariance calculations. The M-values are assumed to be valid at the centre of each bin. The value at the point indicated is then computed from the bilinear interpolation from its surrounding bin values.*

Assume that we seek a value $f(t,u)$ at time t in the range $t_i - \Delta t/2 \le t < t_i + \Delta t/2$, and at argument of latitude u in the range $u_i - \Delta u/2 \le u < u_i - \Delta u/2$, which value is to be interpolated from its surrounding values $M_A = f(t_{i-1}, u_{i-1})$, $M_B = f(t_i, u_{i-1})$, $M_C = f(t_{i-1}, u_i)$, and $M_D = f(t_i, u_i)$ (see **Fig. *20***). Time bins have equal widths of $\Delta t = t_i - t_{i-1}$, and argument of latitude bins have equal widths of $\Delta u = u_i - u_{i-1}$.

The bilinear interpolation formulae used are then:

$$
\begin{aligned}
f_1(t) &= \frac{t - t_{i-1}}{\Delta t}(M_A - M_B) + \left(\frac{3}{2}M_A - \frac{1}{2}M_B\right) \\
f_2(t) &= \frac{t - t_{i-1}}{\Delta t}(M_C - M_D) + \left(\frac{3}{2}M_C - \frac{1}{2}M_D\right) \\
f(t,u) &= \frac{u - u_{i-1}}{\Delta u}(f_2 - f_1) + \left(\frac{3}{2}f_1 - \frac{1}{2}f_2\right)
\end{aligned} \tag{2}
$$

It may be verified that $f(t_{i-1} + \Delta t/2, u_{i-1} + \Delta u/2) = M_A$, and similarly for t and u precisely at the other centered bounding bin values, M_B, M_C, and M_D.

6.3.1 Premise for using sequential overlap statistics as a proxy for error covariance

An oft-cited example of the difference between accuracy and precision is the target analogy as shown in **Fig. 21**. The blue cluster of observations is grouped very tightly; a solution dependent only on the blue observations would yield a precise (consistent and repeatable) solution at the blue diamond that we can see to be inaccurate (biased away from the real condition at the centre of the target), whereas the solution of the second sequence of observations has more noise (imprecise) but accurate (having little systematic bias).

As background to the use of overlap tests as proxy for covariance, note that in order for the blue and yellow ellipses to have significance over a wider population of observations and time sequence of orbital knowledge, they must in absence of unmodeled forces also accommodate the preceding and subsequent orbital solutions (blue and yellow diamonds). By this argument, one can see that the blue error ellipse corresponding to the blue "plus sign" population does not fairly represent and cannot explain the large yellow population diamond outlier solution, whereas the yellow ellipse's imprecision more aptly describes the position of the blue diamond solution for the blue observation set.

Thus, we can see that the precision, not accuracy, is what drives the realism of a "real" covariance; it is the repeatability of the full observational space and orbit solution space which informs us of what our accuracy can be. Said differently, **a system's imprecision sets a lower bound** on what the real accuracy uncertainty would be. Taken over a sufficiently large set of observations and time histories, the precision (of an overlap test) can fairly represent the best accuracy one might expect.

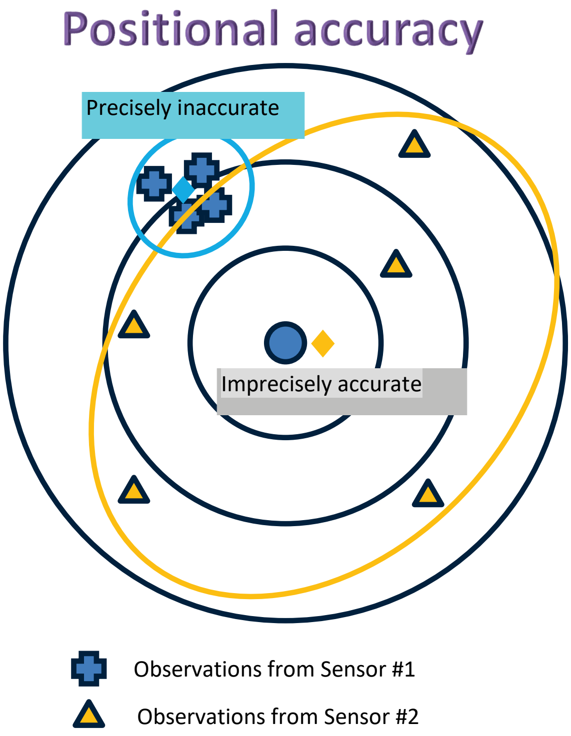

Fig. 21 – *Examples of "precisely inaccurate" and "imprecisely accurate" fusion systems.*

6.3.2 Relationship between sigma span and probability density percentage

COMSPOC's synthetic covariance approach yields 1σ error estimates. It is important to understand what percentage of the true populations such estimates represent in 1D, 2D, or 3D error statistics as a fraction of total, Gaussian, probability density spanning $-n\sigma$ to $+n\sigma$ is dependent on the dimensionality of the space. If a covariance matrix properly represents the ensemble of errors, a prescribed sigma level in one, two or three dimensions should in turn encompass the corresponding percentage of errors shown in ***Fig. 22***, ***Fig. 23***, and ***Fig. 24***, respectively.

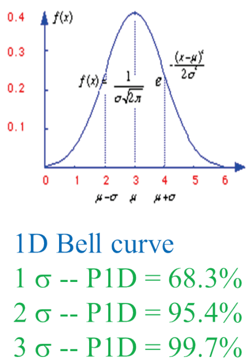

Fig. 22 – One-dim. Gaussian.

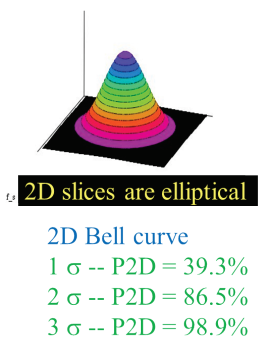

Fig. 23 – Two-dim. Gaussian.

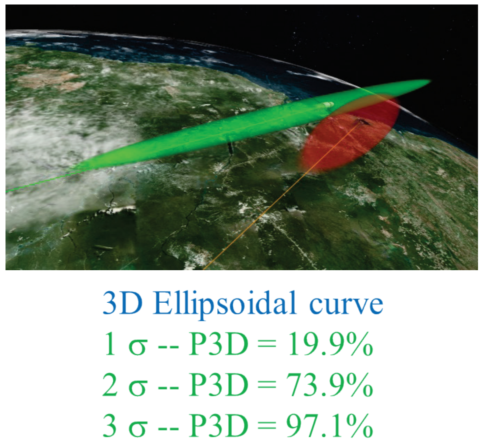

Fig. 24 – Three-dim. Gaussian

While 1σ estimates are critically important to the determination of collision probability, only 20% of the error distribution is contained within a 1σ error ellipsoid; **you are four times more likely to be outside of a three-dimensional 1σ ellipsoid than you are to be inside of it.** It is only when you switch to 3σ ellipsoids that almost all of the population (i.e., 97.1%) have been encapsulated within the error ellipsoid.

6.3.3 Subjective verification of methodology

When an ephemeris and covariance are requested to be generated for a particular satellite at a specified epoch, the SGP4 propagator is invoked for the ephemeris using the latest TLE after the requested epoch. Then the collection of the accumulated difference statistics is used to generate the 21 unique covariance matrix elements (diagonal and upper triangle) at the corresponding propagation times. The ephemeris and covariance are written in the standard Satellite Took Kit (STK) ephemeris file format. The file can then be imported into STK to verify that the displayed uncertainties about the satellite's orbital motion conform to expectations from the understood orbital dynamics. A screenshot of such a display is shown in **Fig. *25***.

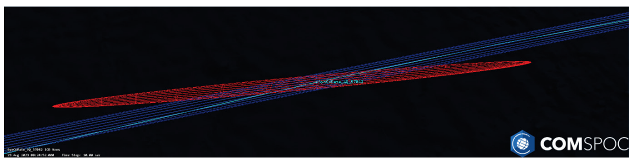

Fig. 25 – *Position and velocity 1-sigma covariance ellipsoids overlaid on the satellite's latest orbit.* *The larger blue ellipsoid corresponds to the position uncertainty, and the smaller red one to the velocity uncertainty. The velocity uncertainty has an arbitrary scale applied to display it in position space.*

This STK visualization depicts the satellite moving through space with two covariance ellipsoids, derived from its synthetic covariance, centred on the satellite's icon. These 1-sigma ellipsoids represent the position covariance (in blue) and velocity covariance (in red), which is scaled by an arbitrary factor to display in position space. (The relative scaling of the ellipsoids has no relevance.) When observing the dynamic propagation of this scenario, the position covariance displays the greatest error in the generally along-track direction, as expected. The position ellipsoid varies smoothly in response to the statistics of the underlying data, shrinking when updated with new TLE data, and growing after the update until the next one.

In this scenario, the velocity covariance (in red) also varied with time and TLE updates. Often its largest axis was oriented significantly farther from along-track direction, even radially outward at times, but with the out-of-plane component the smallest axis, as should be expected from orbital dynamics.

6.3.4 Verification by comparison with other independent estimates of uncertainty

In addition to the initial confirmation of the qualitative appearance and behaviour of the uncertainty ellipsoids, it is worthwhile to compare the statistical results quantitatively to prior findings.

One of the ways to display the results of covariance processing is to display the dimensions for the major, intermediate, and minor axes of the 1-sigma error ellipsoid within the principal eigenvector frame. Position covariance ellipsoid dimensions are produced for each satellite analysed as a standard output of our operational implementation. The title of each plot contains information about the satellite and the median age of the TLEs used to generate its covariance data. Additional statistics on the number and range of TLE ages are also presented.

In these plots, time from epoch is the horizontal axis, starting at the epoch of the latest TLE available, the source of the ephemeris to which the synthetic covariance is to be associated. The vertical axis for the dimensions of the ellipsoid is a logarithmic scale in kilometres. An example is given below in **Fig. *26*** for the passive geodetic satellite, Stella (NORAD ID 22824), which was launched into a sun-synchronous orbit in 1993. Stella has a low area to mass ratio, with a mass of 48 kg and a diameter of 24 cm. This object was chosen here to serve as a reference for comparison with existing statistical results by (Mason, 2009) [12].

Notable in **Fig. *26*** is the expected along-track uncertainty dominance, though the overall relative size of this ellipsoid is small compared with many other results within the LEO orbit regime (see Appendix 1). This may be due to the importance of the measurements of this geodetic satellite and a corresponding increase in surveillance network tasking. It can be seen from the median age of the TLEs going into the generation of this plot (0.71 days) that this satellite's position is updated frequently.

In the prior study by (Mason, 2009[12]), residuals were calculated between the ephemerides generated by SGP4 using TLEs and the high-accuracy Precision Orbit Ephemeris generated by the Center for Space Research of the University of Texas, Austin. We note in figure 3-2, page 27, of that work a plot of the mean of the residuals in the along-track direction (denoted *transverse* in that work), generated for a conveniently commensurate length of 7 days, as in our own study. The along-track mean residual value is sub-kilometre for this span, which is quite similar to the results in our study, shown in the figure with a maximum of around 0.4 km.

Comparisons were also made with the analysis of TLE propagation uncertainties of satellites within the GPS constellation done by (Kelso, 2007) [[13]]. The statistics of internal consistency within propagations from different TLEs are shown for the GPS satellite designed PRN11 in their study, corresponding to NAVSTAR 46. In [13], assuming that the difference range represents the entire 3-sigma spread, the 1-sigma value was inferred as around one third of the range, or 0.8 km, which matched nicely with the sub-kilometre 1-sigma dimension for that same satellite from our method.

An indirect comparison was made with the U.S. Department of Commerce "GEO/MEO Pilot initiative and the technical performance assessment and comparative study[14] generated in support of the Pilot. In that assessment, **Fig. *27*** depicts the median (or 50th percentile) absolute accuracies for a variety of Space Situational Awareness positional products, including TLEs and SP. In comparison, **Fig. *28*** and **Fig. *29*** characterize the major, intermediate, and minor principal eigenvalue 1σ (or 68.3rd percentile along the relative position vector direction) values for TLEs and SP ephemerides, respectively.

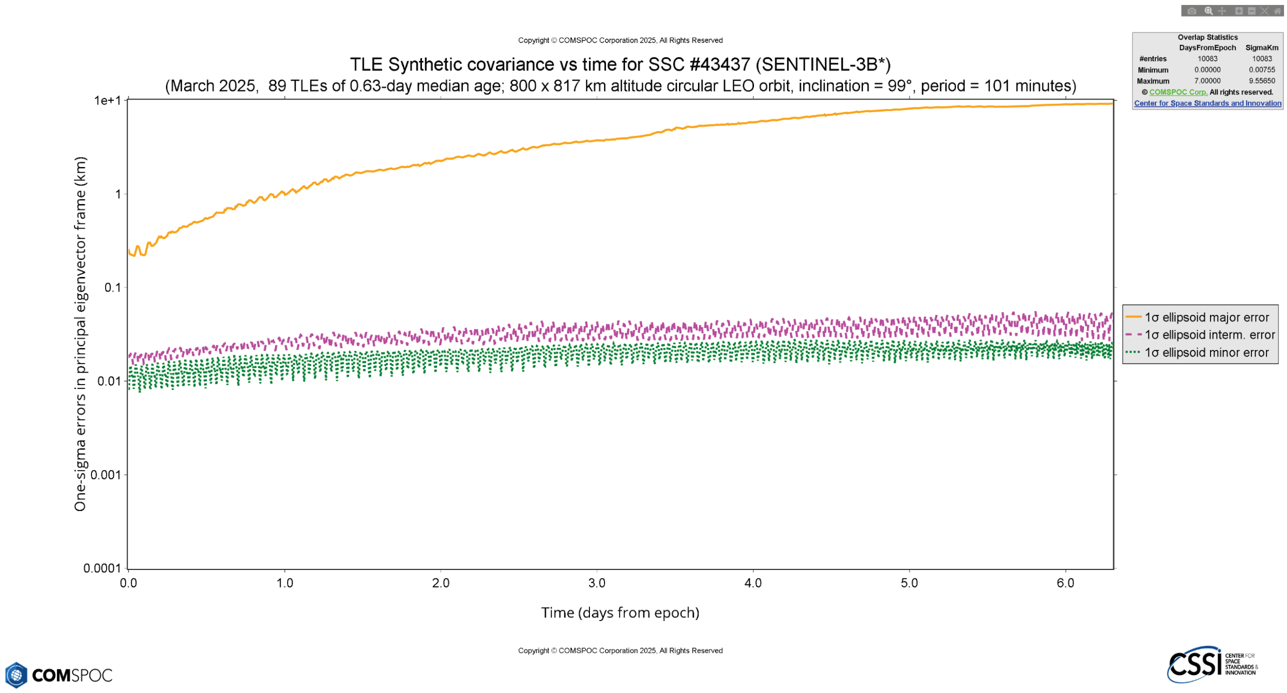

Fig. 26 – *Example of the one-sigma ellipsoid dimensions plot from the synthetic covariance generated for Sentinel-3B,* *a European Space Agency Earth observation satellite dedicated to oceanography in a sun-synchronous LEO orbit. The asterisk (*) following the name indicates that this estimated to be an active spacecraft.*

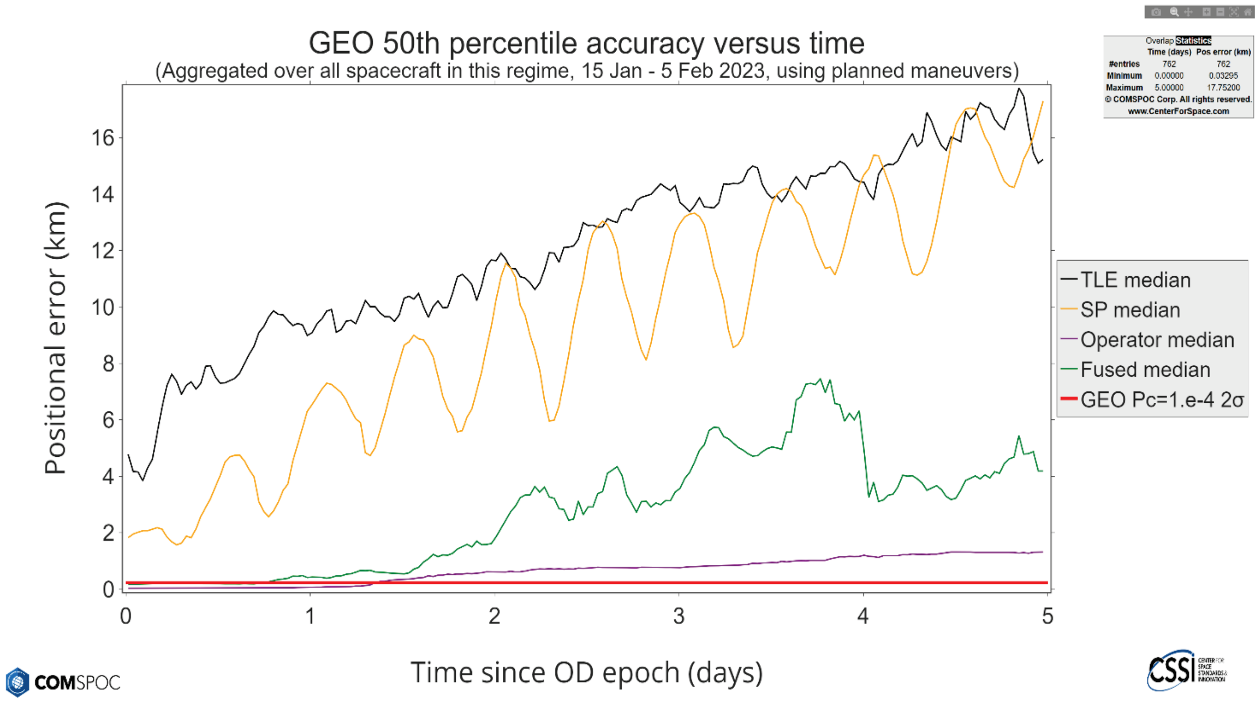

Fig. 27 – *Median (or 50th percentile, i.e., "typical") orbital accuracies for TLEs, SP, and other products* *as compared to independent reference ephemerides for 6 GEO and 6 MEO spacecraft.*

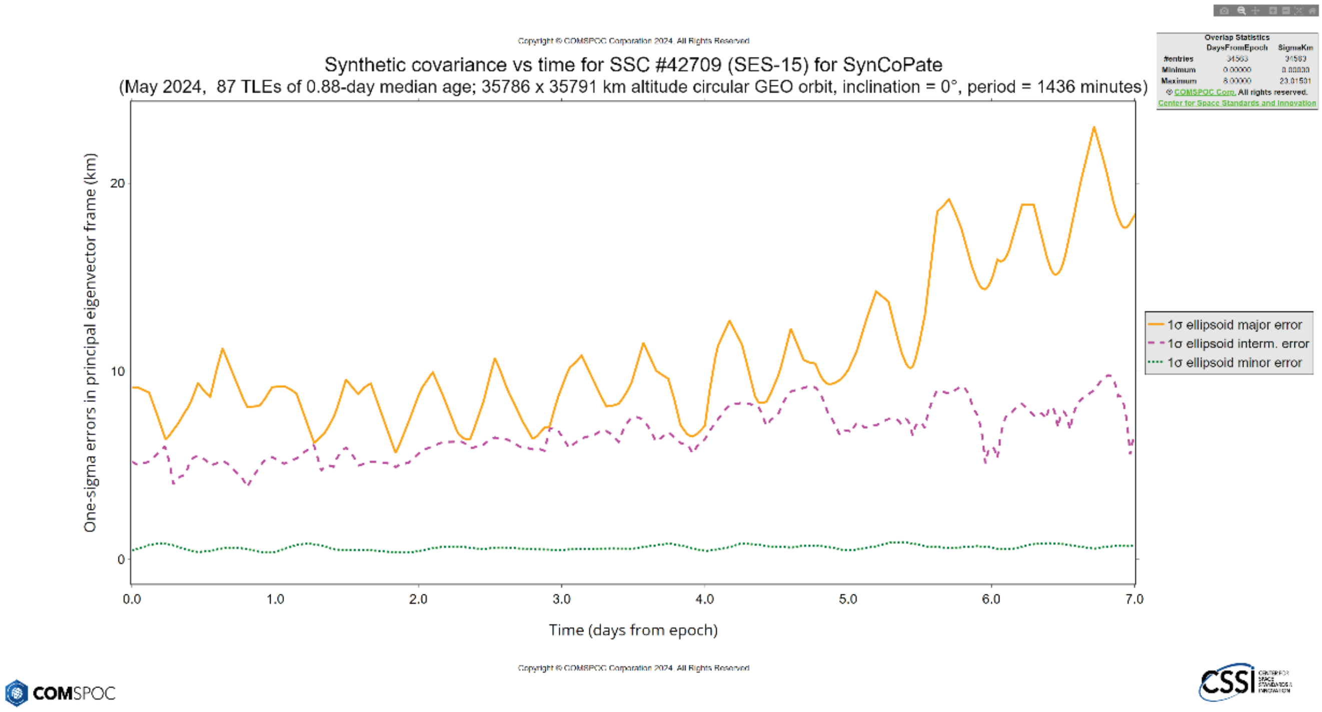

Fig. 28 – *TLE 1σ (or 68.3rd percentile) major, intermediate, and minor principal eigenvalue sigmas for SES-15.*

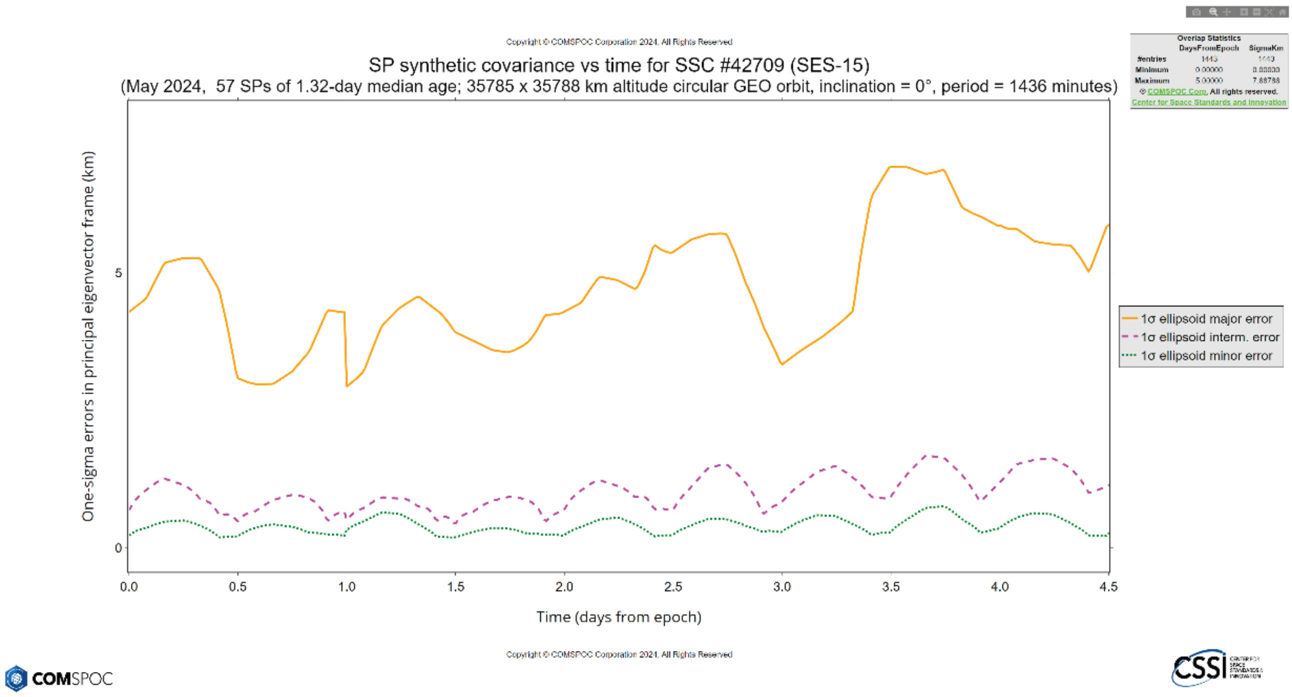

Fig. 29 – *SP 1σ (or 68.3rd percentile) major, intermediate, and minor principal eigenvalue sigmas for SES-15.*

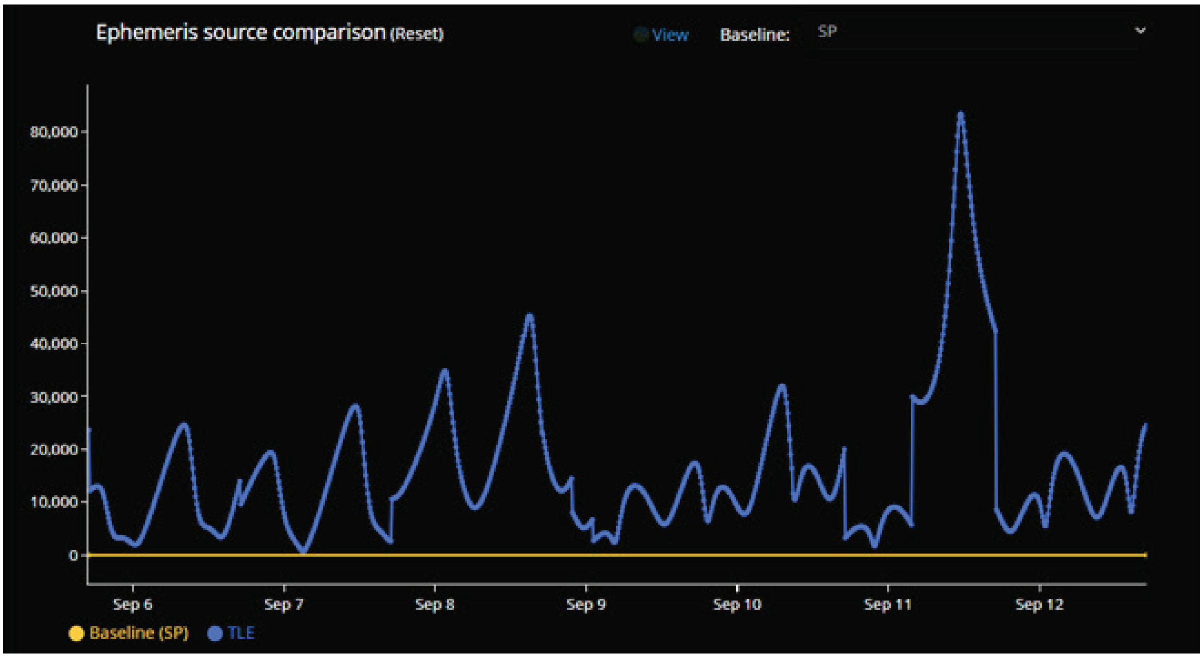

Fig. 30 – *Comparative SSA between a reference (here adopting SP as the baseline) and an SSA product (e.g., TLE).* *In this case, the positional difference is shown [metres].*

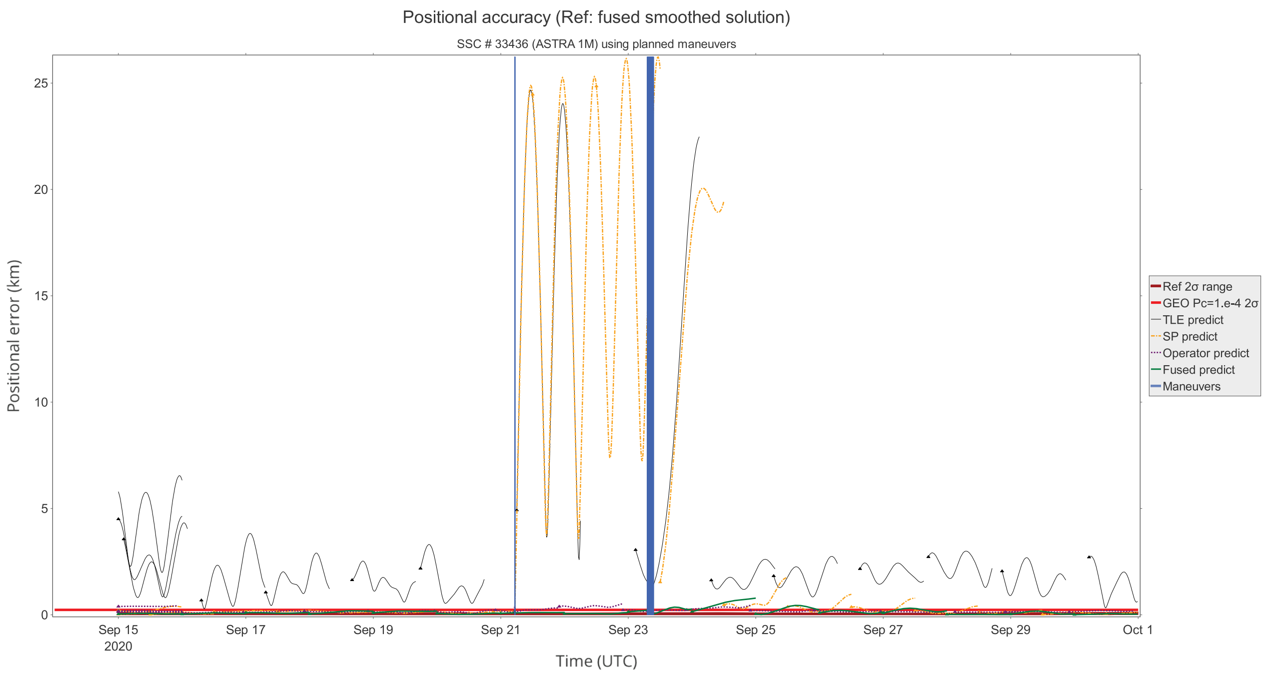

Fig. 31 – *Example of STCM demonstration predict accuracy on a linear y-axis scale.*

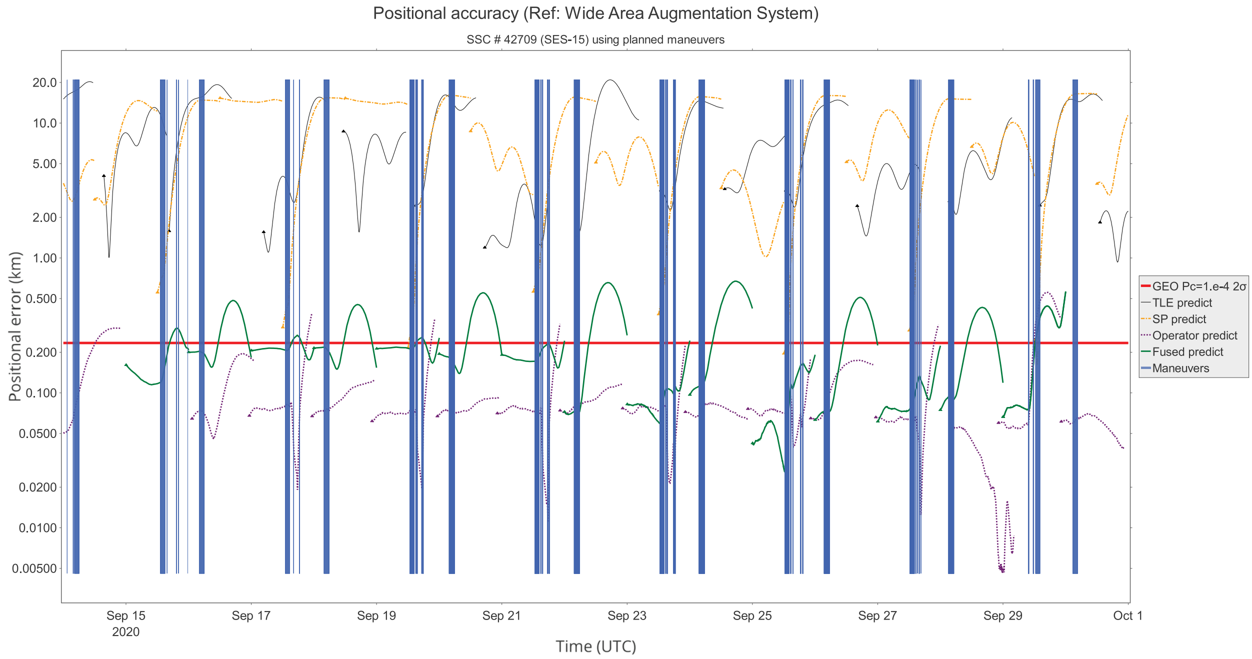

Fig. 32 – ***Example of comparative SSA measured against an independent "truth" orbit (WAAS).***

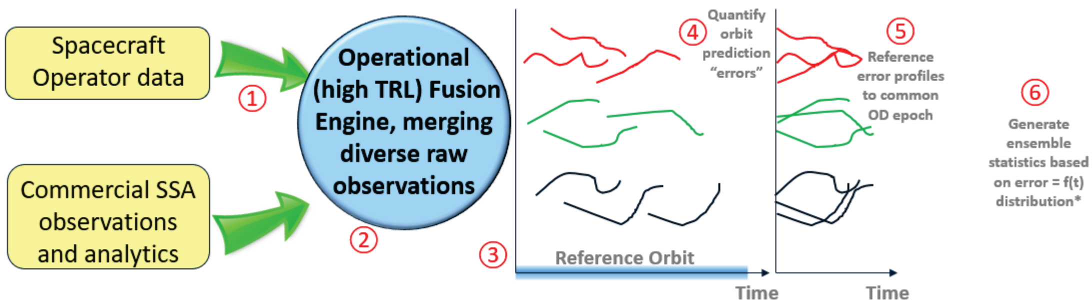

Fig. 33 – ***Performance aggregation by SSA product type (red vs green vs black) as a function of prediction time.***

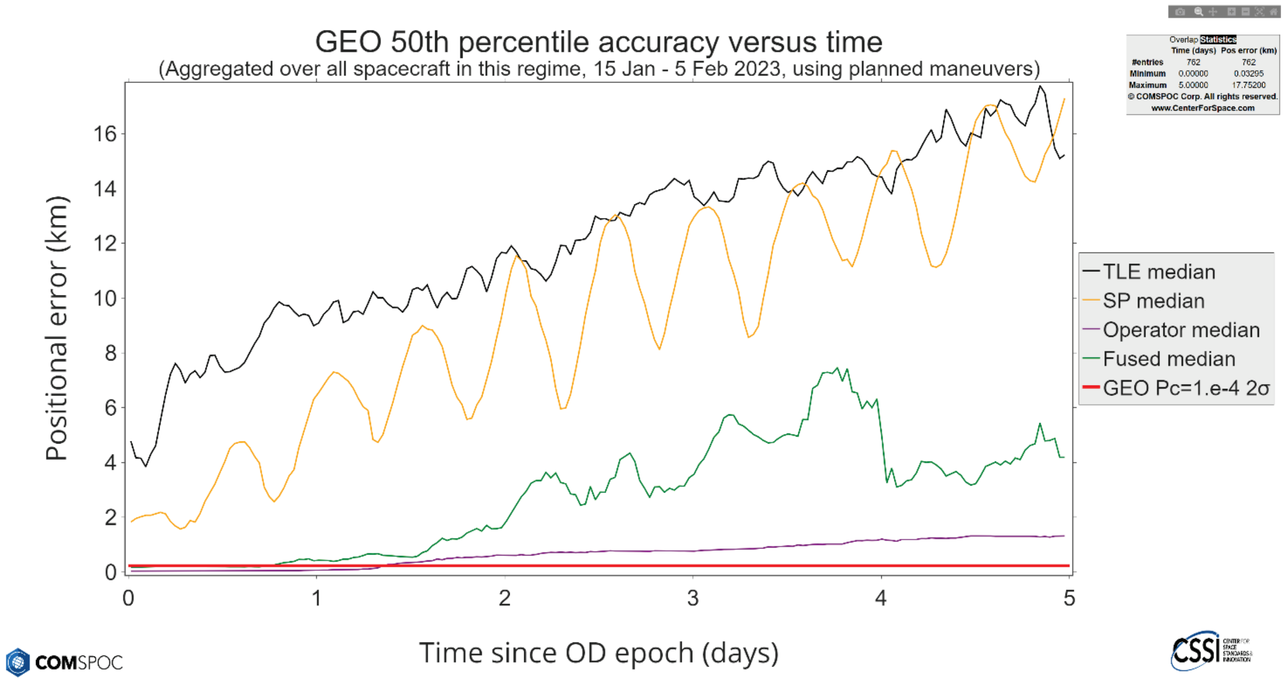

Fig. 34 – *Typical accuracy of a variety of SSA products aggregated across six GEO independent 3rd party reference spacecraft (linear accuracy scale).*

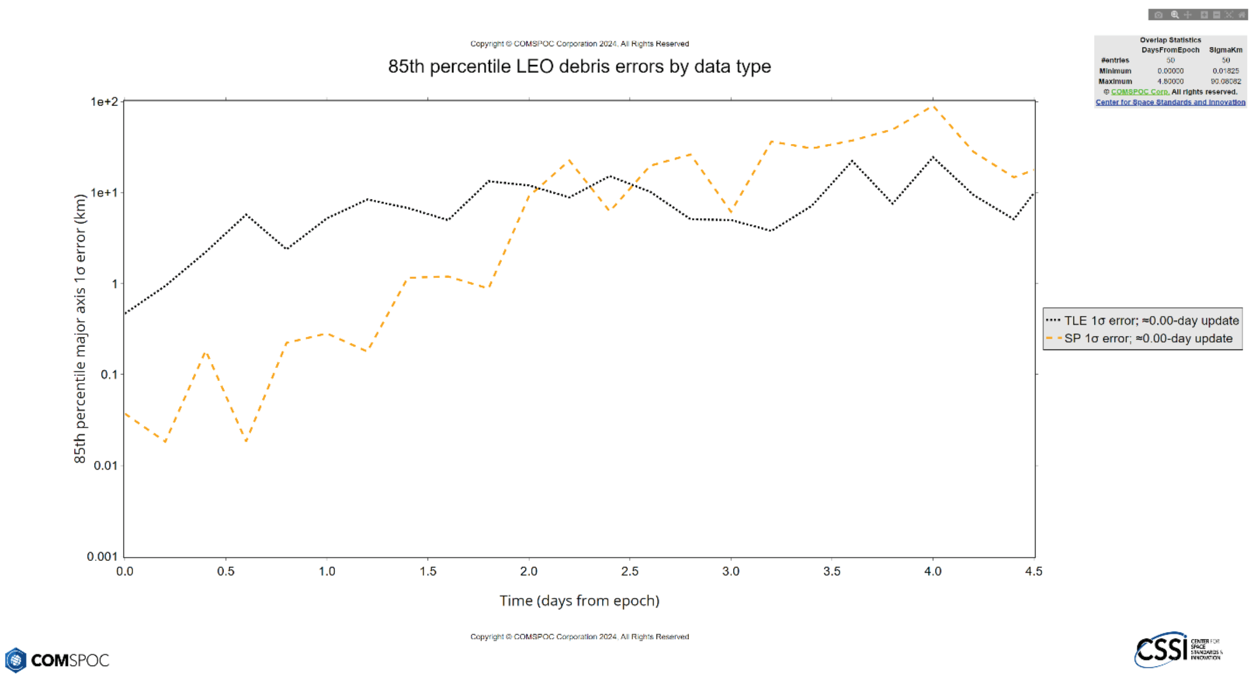

Fig. 35 – *Major 1σ error of TLE (black) and SP SSA for DEBRIS objects.*

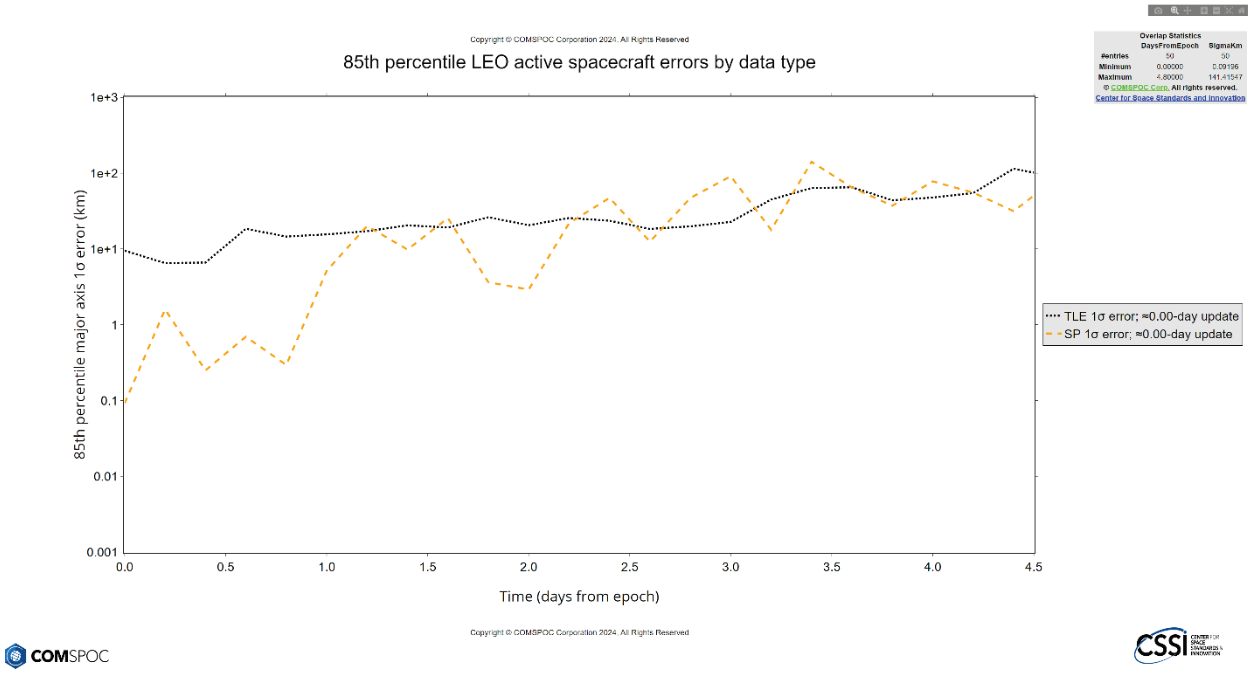

Fig. 36 – ***Major 1σ error of TLE (black) and SP SSA for ACTIVE spacecraft.***

Since these percentiles are not fully harmonized, concrete conclusions regarding consistency between the GEO/MEO Pilot assessment and synthetic covariance for this sample GEO spacecraft cannot be drawn. Yet it is apparent that the trends and magnitudes are reasonably well aligned: where the GEO/MEO Pilot found GEO major eigenvalue TLE median errors trending upwards from ≈ 4 to 17 km over 5 days and GEO SP median errors trending upwards from ≈ 2 – 16 km, synthetic covariances generated for SES-15 had 1 σ (or 68.3rd percentile) errors trending upwards from ≈ 5 to 14 km over 5 days and GEO SP median errors trending upwards from ≈ 3 – 8 km.

Today, the COMSPOC "Synthetic Covariance Partites" (SynCoPate) tool runs as a daily automated process and has been generating synthetic covariances for TLEs and SP data for a year now. Publicly available catalogs containing approximately 26,000 objects are downloaded at a frequency of 12 times per day for TLEs and once per day for SP data. The statistical accumulation of difference data is stored for each 7-day period (referred to above as an *era*) as individual binary files for each satellite, accessible by a memory map within the operational program. If a TLE is updated, it will be designated the new 'truth', and this will trigger a new set of differences to be formed with prior TLEs. The differences will be added to the existing difference data when the program is running in maintenance mode. This type of run can be completed in several hours.

To the best of our knowledge, this is the world's first operational time- and argument-of-latitude-binned synthetic covariance tool spanning TLEs, SP, and O/O ephemerides, yielding operationally relevant covariance information where none existed previously.

7 Comparative SSA information

"Comparative SSA" as we've defined it is nothing more than comparing multiple versions or ensembles of SSA products with each other to facilitate greater understanding and search for patterns in the behaviour of accuracy, timeliness, completeness, etc. In its elemental form, one can for example compare orbit positional knowledge (whether historical or predictive, as shown in **Fig.** ***30***), conjunction prediction results, collision probability estimates, etc.

Ideally, one seeks to compare each SSA product versus some notion of an independent third-party "truth" reference orbit trajectory. Unfortunately, very little truly independent 3rd-party orbit information exists. In most cases where good reference orbits are unavailable, orbit determination processes that use Extended Kalman Filter (or more generally, a "sequential filter") technology typically employ a "filter" and a "smoother" stage, and the resultant smoothed ephemeris can be often used as a sufficiently accurate approximation of "truth".

Reference orbits have errors also, although they are typically much smaller than the errors extant in other SSA products such that legitimate estimations of the other SSA products' errors can be determined by simply differencing the trajectories as shown in **Fig.** ***31*** [15]. In this figure, TLE accuracy is shown in black, SP in dashed-line yellow, spacecraft Owner/Operators (O/O) in dotted purple, and COMSPOC fused solution (developed in deep collaboration with O/Os) in solid green. Maneuvers are shown as vertical blue bars (with the width denoting duration). O/O ephemerides and COMSPOC fused solutions are seen to be several orders of magnitude more accurate than TLE or High Accuracy Catalog (HAC) SP products, largely driven by the inability of TLEs, SP, and the underlying legacy SSA software to accommodate maneuvers.

The wide variability in accuracy of SSA products often forces us to switch from the linear y-axis scale of **Fig. *30*** and **Fig. *31*** to a logarithmic y-axis scale as shown in **Fig. *32*** [15] in an effort to clarify the relationships between various SSA products. But a caution must accompany the use of logarithmic scales: While the logarithmic scale allows all data to be clearly shown on a single plot, the log scale tends to deemphasize large positional errors while exacerbating small ones.

Comparative SSA processes allow the analyst to determine if SSA data is "fit for the purpose" of space flight safety. From a flight safety standpoint, there exist a wide variety of conjunction assessment screening metrics [15]. The choice of metric often depends on the orbit regime and its associated threat profile, operator staffing, maneuver prolusion capability and resources, etc. For any such conjunction assessment metric to be operationally relevant and viable, the accuracy of SSA data must be sufficient to support the selected collision avoidance maneuver "Go-No Go" threshold. It is incumbent upon each operator to ascertain what accuracy the SSA data needs to have to ensure that their flight safety processes are operationally relevant and effective.

While the above plots are certainly of interest for specific spacecraft of interest, it is of far greater interest to understand the performance of each SSA product averaged over time, and within certain orbit regimes and/or manoeuvrability categories [16]. Statistics can be aggregated as shown in **Fig. *33*** to produce error statistics within each category as shown in **Fig. *34***. This figure demonstrates the value of comparative SSA products in determining whether a given product is fit for purpose.

Since "truth" reference orbits that are truly independent from the SSA system (i.e., not used for system calibration) are rare, synthetic covariance information provides a more comprehensive window into the comparative performance of a variety of SSA products. The following results have been aggregated to determine the precision corresponding to an arbitrary percentile of interest. **Fig. *35*** is an aggregation of TLE and SP 85th percentile overlap precision for all LEO debris objects (below 2000 km). It is readily seen that SP data is substantially better for debris objects at orbit epoch, but after several days, TLEs are more precise than SP, presumably due to the TLE fitting long-term perturbations using averaged quantities. This is not the first time that this effect has been observed; this was also seen in the STCM demonstration and the GEO/MEO Pilot activity.

As seen in **Fig. *36***, the 85th percentile prediction accuracy of active spacecraft is substantially worse than that for debris objects (although the shape of the lines is roughly similar, note that the y-axis scale is much bigger in **Fig. *36*** than it was in **Fig. *35***). COMSPOC's CSSI 2023 research (freely available on the Spacebook website) is entirely consistent with this finding, indicating that spacecraft maneuvers represent the single largest degradation in SSA. While this explains the thinking behind the Space Data Association's foundational use of operator data to address such positional errors, that path is not always reliable, e.g., if the operator is not able to obtain an accurate OD solution or propagate their orbit accurately, or if the operator is unwilling or unable to cooperate with a flight safety system by sharing their data.

8 XP-TLEs fit to SP ephemeris

SGP4-XP is a new semianalytical orbit theory available to the public through the United States Space Force (USSF) dynamic link library (.DLL) on the Space-Track.org website. While this propagator improves upon the venerable SGP4 Two-Line Element (TLE) set orbit propagator originally developed in the 1970s in all orbital regimes, it performs much better in GEO.

SGP4-XP has more realistic force models that are particularly well-suited for all orbit regimes to include the gravitational resonance terms in GEO. The new theory [signified by a message type of "4" in the TLE] also accommodates the ballistic coefficient for atmospheric drag (i.e., C_DA/m, where C_D = the drag coefficient, A = average cross-sectional area, and m=mass), and Solar Radiation Pressure (SRP), i.e., $A\,\gamma\,/\,m$, where γ = surface reflectivity and A and m are defined as before. These new coefficients, occupy the TLE fields formerly used by SGP's Bstar and mean motion double dot, respectively.

Beyond those changes to the TLE fields, the other difference is that the element set ephemeris type (which has always been 0 for SGP4) is now set to 4 to designate this as an SGP4-XP element set.

Because SGP4-XP is a semianalytical model that incorporates refined perturbation models, positional accuracy can be significantly more accurate (anecdotally, perhaps a five or ten-fold improvement) than the older SGP4 TLEs. But note that these new SGP4-XP TLEs are *only* compatible with the USSF SGP4-XP DLL library.

Spacebook optimally fits SGP4-XP TLEs to ephemerides (obtained from any source, but in this case, SP ephemerides are used) via a simple differential correction scheme. Users who have the USSF SGP4-XP software DLL library may find these SGP4-XP TLEs useful for routine operations, as they do have improved accuracy over standard TLEs.

9 Augmented DISCOS data

ESA's excellent DISCOS database [17] provides an excellent resource for obtaining spacecraft dimensions, mass, and cross-sectional area. Such information is essential for the evaluation of atmospheric drag forces, collision probabilities, and collision consequence (e.g., the expected number and masses of fragments produced.

Spacebook shares an augmented set of information by additionally estimating the median Hard Body Radii (HBR) and median cross-sectional area values. Median, or 50^{th} percentile, values tend to do a better job of representing "typical" conditions within an ensemble set than an average value does. The methodology for computing such median values is contained in [18].

When performing conjunction analysis, it is often the case that the orientation and configuration/shape of the satellites are unknown. It is almost exclusively the case for debris objects. This necessitates certain assumptions when computing collision probability. A common practice is to approximate a spacecraft's hardbody with an encapsulating sphere. This one-shape-fits-all approach eliminates the need to determine orientation, but results in an overestimated object volume and an overinflated probability unless both satellites are actually spheres.

To produce more representative probabilities, we use a satellite's dimensions to define a rectangular box. This more accurately portrays the actual collision threat by projecting a smaller area than a sphere, the downside is that the box's orientation must be known. To address this, we provide a spectrum of values for all possible orientations based on uniformly spaced viewing angles. The user then has the freedom to choose a suitable range of orientations. Even when choosing the maximum footprint possible, the resulting probability of the box will be less than that of the sphere.

Fig. 37 shows a box of length (l), width (w), height (h) with Aeolus dimensions of [13m, 4.3m, 1.6m] (https://discosweb.esoc.esa.int/, subscription required) placed inside a sphere populated with evenly spaced viewing points. For what follows, it is always assumed that $l \geq w \geq h$.

The first step in this sampling process is to generate equally distributed viewing points on the surface of a sphere to observe a rectangular box. The three-dimensional box is viewed from all points to determine the associated two-dimensional, projected, surface areas as they would appear in a probability encounter plane. These resulting areas are then sorted in ascending order and their cumulative representation displayed as a monotonically increasing distribution in **Fig. 38**.

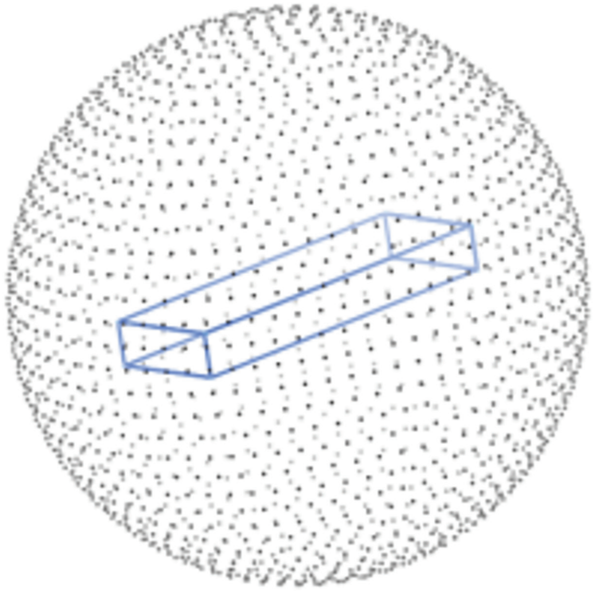

Fig. 37 – *Box surrounded by equally-spaced viewing points*

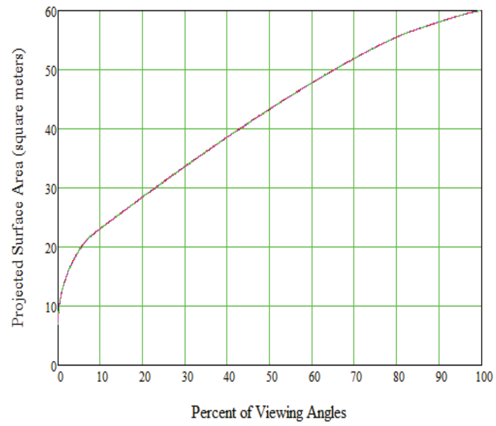

Fig. 38 – *Aeolus area projections*

As shown in **Fig. 38**, 80% of the viewing angles will observe a surface area at or below $56m^2$, 50% below $44m^2$, and so on. The associated radii for representative circles in the encounter plane are computed using a method similar to Chan's Method of Equivalent Cross-Sectional Area (MECSA)[19]. Unlike Xie and Chan's approach, the rectangular dimensions and orientation are redefined in the encounter plane rather than converting to a circle, thus simplifying the integrable region. The resulting radius distribution is shown in **Fig. 39**.

From **Fig. 38** and **Fig. 39**, we see that the box's largest projected area is $60m^2$ which will produce a circle of equivalent area with radius of 4.37m.

To contrast this with a satellite's representation as an encapsulating sphere, **Fig. 40** shows a sphere of minimal volume that touches all corners of the same Aeolus box.

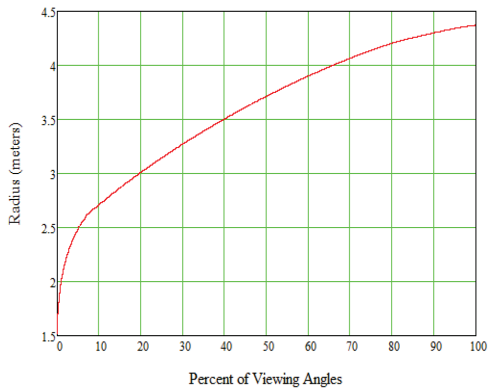

Fig. 39 – ***Equivalent radii of Aeolus area projections***

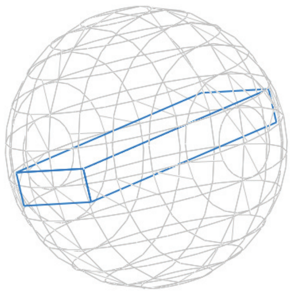

Fig. 40 – ***Sphere of minimal volume touching all corners of box***

The sphere's diameter is 6.89m with a projected area of 149.3 m^2 regardless of viewing angle. In the encounter plane, such a circle will envelop the largest possible Aeolus box plus an additional 89.3 m^2 of density space. Thus, for the same centroid, the box's smaller footprint will produce a lower and more reasonable probability. This holds true for all cases because the encapsulating circle will always contain more probability density space than a box's projected maximum area.

The minimum, maximum, and/or user-choice percentages of the box are used to establish their respective radii. When modelling an encapsulating sphere, its radius is used instead. Summing the radii for both conjuncting objects yields the combined hardbody radii (CHBRs) for all 3 cases.

10 Downloading Spacebook via the UI and API

The core functionality of Spacebook is the ability to download space data to use in your own missions or applications. There are two ways to download data: through the user interface or through the API.

10.1 Downloading from the User Interface

The user can select the Downloads card on the Spacebook home page to open the download window as shown in **Fig.** ***48***. In the upper section of the page, the user can run bulk downloads for TLE, space weather, EOP, and satellite catalog files. To download a bulk set of data, click one of the options on the right side of the window in that row.

In the bottom section of the window, the user can download TLE-based ephemeris with synthetic covariance, a graph of the synthetic covariance, and an XP-TLE for each object. The list of satellites can be filtered in the same way as the catalog search page. To download ephemeris with synthetic covariance, click the down arrow under that column. To download a graph of the synthetic covariance, click the graph icon under the synthetic covariance column. To download XP-TLEs, click the down arrow under that column. Some objects also have reference ephemeris, which can be downloaded if the download icon is present under the reference ephemeris column for that object.

10.2 Downloading from the API

For individual downloads, you can get the web endpoints for the API by hovering your cursor over any of the download icons. The endpoint will be displayed in the lower left corner of the window.

10.2.1 Bulk download endpoints

Spacebook's bulk download endpoints are as follows:

- TLE: https://spacebook.comspoc.com/api/entity/tle
- Space Weather Full: https://spacebook.comspoc.com/api/spaceweather/full
- Space Weather Recent: https://spacebook.comspoc.com/api/spaceweather/recent
- EOP Full: https://spacebook.comspoc.com/api/eop/full
- EOP Recent: https://spacebook.comspoc.com/api/eop/recent
- Satellite Catalog SD file: https://spacebook.comspoc.com/api/entity/satcat/sd
- Satellite Catalog CSV file: https://spacebook.comspoc.com/api/entity/satcat/csv
- Satellite Catalog JSON file: https://spacebook.comspoc.com/api/entity/satcat

10.2.2 Object GUIDs

The API for individual object data requires a unique GUID which Spacebook has assigned to each object. The format for the endpoints is:

- TLE-based ephemeris with synthetic covariance: https://spacebook.comspoc.com/api/Entity/synthetic-covariance/GUID

- Synthetic covariance graph: https://spacebook.comspoc.com/api/Entity/synthetic-covariance-plotly/GUID
- XP-TLE: https://spacebook.comspoc.com/api/Entity/xp-tle/GUID
- Reference ephemeris: https://spacebook.comspoc.com/api/Entity/reference-ephemerides/GUID
- Reference ephemeris OCM format: https://spacebook.comspoc.com/api/Entity/reference-ephemerides/ocm/GUID

The unique GUID for each object can be found in the Satellite Catalog JSON file in the "id" field. Note that when looking up objects in the JSON file by SSC, the file does not use leading zeros for the SSC field. The GUID for an object can also be found in the Satellite Catalog CSV file under the COMSPOC_ID column.

11 Spacebook Explorer

A key component of the web-based Spacebook portal is its high-performance, CesiumJS-based Explorer. Spacebook Explorer is a tailorable 3D visualization engine that provides a current view of space activities and visualizes space traffic in real time. Advances in client-side rendering and open standards enable time-dynamic volumetric visualization of orbital traffic and debris density, enhancing situational awareness and safety.

11.1 CesiumJS: High-Performance Visualization

CesiumJS is an open-source JavaScript library for rendering precise, interactive 3D globes and maps. Its ability to visualize massive, time-dynamic geospatial datasets makes it ideal for aerospace applications, including space situational awareness. Signification benefits include:

- Accessibility: Built on WebGL, CesiumJS runs in any modern browser, making applications accessible across desktops, laptops, and mobile devices without requiring heavy desktop workflows.
- Precision and Scalability: Designed for aerospace use, CesiumJS supports high-accuracy spatial and temporal visualizations, making it well-suited for large-scale datasets and real-time analysis.
- Interoperability: Streams data from multiple sources, integrating 3D Tiles with industry-standard formats for seamless geospatial visualization.

The default Spacebook Explorer window shows all space objects in the current Spacebook catalog. Each dot represents a space object and is coloured according to the following default scheme:

- Active satellites – green
- Rocket bodies – red
- Inactive satellites – yellow
- Debris – grey
- Unknown – white

11.2 Controlling the view

To control the view in the globe window, left-click and drag to rotate the globe and right-click and drag to zoom in and out (alternatively, you can use the scroll wheel on the mouse to zoom).

11.3 The object window

Click on any of the objects to bring up its object window as shown in **Fig. *45***. The object window provides information and display controls for the currently selected object. You can reposition the object window by clicking on the cross arrows in the upper left of the window and dragging. Click on the X in the upper right corner of the window to dismiss it. The window comprises three tabs: Info, Position Data, and Customize.

The Info tab contains asset information about the object from the Spacebook catalog.

You can use the controls on the Position Data tab to switch between showing the dot at its SGP4 location and showing the dot with synthetic covariance — using the COMSPOC TLE-based ephemeris with synthetic covariance. Select **Show Orbit** to turn on the object's orbit as drawn in inertial space. Select **Track Object** to zoom to the object in the Explorer window.

The customize tab provides controls that enable you to change the appearance of the dot representing the object in the Explorer window.

11.4 Catalog search

The user can refine the display of space objects in the Explorer by using the catalog search tool, which appears as a keyword terms box and magnifying glass icon in the upper centre of the Explorer window.

The entire catalog can be searched by typing anything into the keyword terms box. Specific data fields can also be searched, including NORAD id, international id, name, status, owner, launch site, launch date, apogee, perigee, period, inclination, or RCS. To search by a data field, click the open box beneath the column header. Some of these will allow you to type any text (such as name or id number), whereas some of these will display a list of check boxes that allow you to filter on that column (such as status or owner). **Fig. *46*** illustrates an example search in which a user has filtered down to only the spacecraft owned by Brazil that were launched since January 1, 2010.

11.5 Creating themes in Spacebook

The user can change the theme of all the objects that are the result of your filters by clicking the Bulk theme button at the top right of the catalog search page. Here the colour and size of the dots can be changed in the Explorer window for all objects remaining in the filter results window. All of these objects can then be assigned to a group by clicking the left facing arrow to send them to the group box.

11.6 Groups

A group is a selection of objects in the Explorer window that share visualization settings. Objects can be added to a group by filtering the list to display the objects wanted in the group and then clicking the left-facing arrow in the middle of the catalog search window. Objects can be removed from the group by filtering within the group box on the left of the catalog search window and clicking the right-facing arrow. The properties window for the group will be displayed in the bottom right corner of the Explorer window.

11.7 The group window

The group window indicates the number of objects in the group and lists them — by default, by international ID and name. The members of the group and their visualization properties can be changed using the three icons above the list and clicking on the eye icon to restrict the display of objects in the Explorer window to only objects in the group. Clicking the gear icon reopens the catalog search page to modify the members of the group. Clicking the palette icon changes the theme — i.e., the colour and size of the dots — of all objects in the group. The Explorer window in **Fig.** *47* has been filtered to show only the objects in the group window, with the theme for the group objects set to orange, size 20 dots.

Whenever a change is made to the visualization, the Explorer displays an indicator in the upper middle area of the window indicating a change. Clicking the X next to this indicator resets the visualization settings of the Explorer.

11.8 Saving themes

By signing up for a free Spacebook account, the user can save group and theme settings to their profile for ease of use and retrieval later. Clicking the palette icon in the upper right corner of the window saves the theme, which will open the theme manager where the user can name them and save it. Themes can be loaded by opening the theme manager and clicking on the menu in the lower half of the window.

12 Visualizing Orbital Traffic with 3D Tiles and Voxels

Sometimes, a volumetric depiction of activities in space makes more sense. Consider regions of space where communications is degraded due to Electro-Magnetic Interference (EMI), or sensor fields-of-view and -regard, spatial density depictions for RSOs, or fragmentation clouds caused by collision (e.g., **Fig.** *41*), explosion, or intentional fragmentation (ASAT, **Fig.** *42*). P

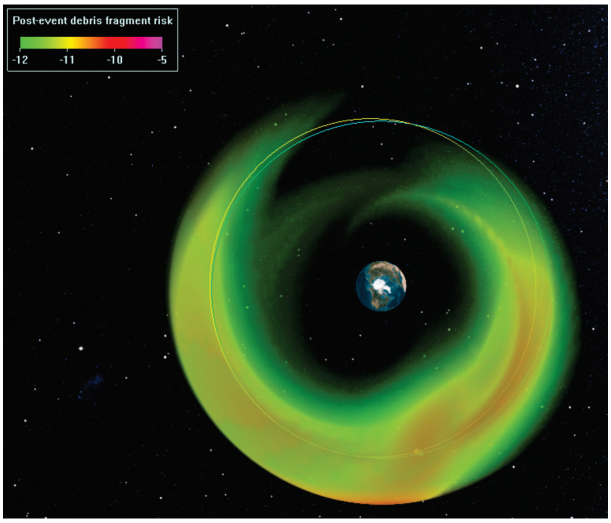

Fig. 41 – ***Volumetric display in the aftermath of an accidental collision in the GEO belt.***

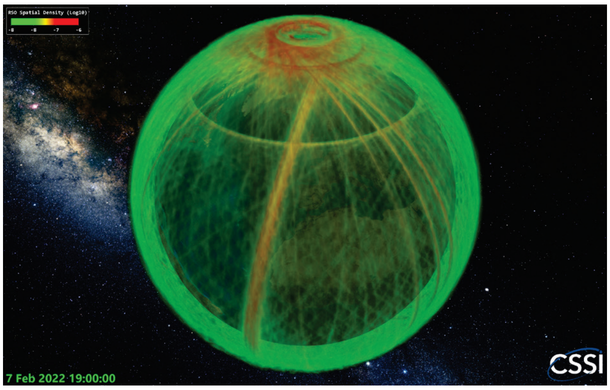

Fig. 42 – ***Volumetric display in the aftermath of the Russian ASAT test conducted 15 Nov 2021.***

12.1 Cesium voxel rendering with ray marching

The CesiumJS tool provides the backbone of Spacebook's visualization capabilities. CesiumJS can now also render 3D volumetric datasets using voxel rendering with raymarching. Unlike mesh-based approaches like Minecraft, raymarching supports translucency, real-time colour mapping, and metadata-based filtering.

3D Tiles, an open standard widely used by companies like Google to stream massive photorealistic 3D data, efficiently renders large datasets across platforms. Built on glTF, a widely adopted open 3D standard, 3D Tiles benefits from this robust ecosystem.

A key challenge in SSA is representing and analysing space object density over time. A proposed voxel extension for 3D Tiles enables:

- Efficient Streaming and Accessibility: 3D Tiles optimizes large-scale space object density visualizations for web-based access.
- 3D Tiles and glTF Voxel Extensions: Uses implicit shape definitions and gridded voxel data to store volumetric data efficiently. These extensions have been explored in subsurface, undersea, and aerospace applications to validate feasibility across industries.
- Time-Dynamic Density Mapping: The 3D Tiles voxel extension allows mapping of space object density to user-defined colour gradients and translucency in real time, improving interpretability and decision-making for space traffic visualization.

With Cesium's new volumetric voxel rendering, discrete "dot" animations such as is shown in **Fig.** ***45***) can now be replaced by point cloud depictions (***Fig. 43***) or further enhanced by voxel rendering (***Fig. 44***).

12.2 Data pipeline steps for space object density visualization

1. **Data Ingestion and Transformation**: Parsing time-based samples and converting celestial frame positions (ICRF) into a static geographic coordinate system using Earth orientation parameters (EOP).
2. **Grid Generation**: Establishing a 3D voxel grid based on sample distribution.
3. **Spatial-Temporal Density** Approximation: Using Inverse Distance Weighting (IDW) to interpolate data spatially across the voxel grid. Timestamped density data for each voxel is fitted using Polynomial Regression to model density variations over time.
4. **3D Tiles Authoring**: Preprocessing optimizes runtime visualization by encoding hierarchical levels of detail in 3D Tiles using the 3DTILES_content_voxels draft extension. Polynomial coefficients are stored in glTF binary buffers using the EXT_primitive_voxels draft extension.
5. **GPU-Optimized Rendering**: At runtime, voxel density values are computed dynamically on the GPU, mapped to a colour gradient and translucency scale for clear visualization. Users can adjust colour gradients, translucency, and filter data by spatial extent or value range.

12.3 Sample application of CesiumJS to volumetric displays

To explore the efficacy of incorporating such volumetric displays into Spacebook, COMSPOC generated sample breakup data corresponding to a mid-December DMSP breakup (fragments labelled as "DMSP 5D-2 F14 DEB" in the SATCAT) and then worked with their Cesium partner to transfer that data to the Cesium team to process and render.

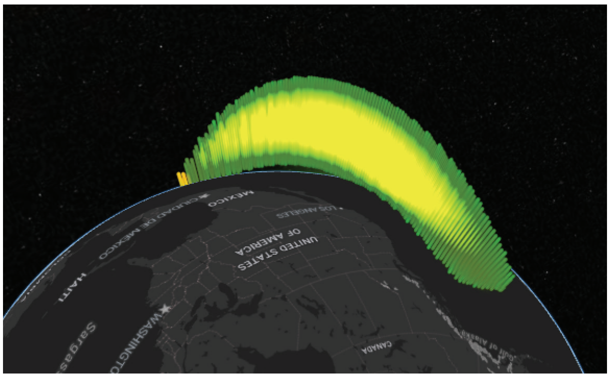

Fig. 43 **– Cesium point cloud display in the aftermath of an accidental collision in the GEO belt.**

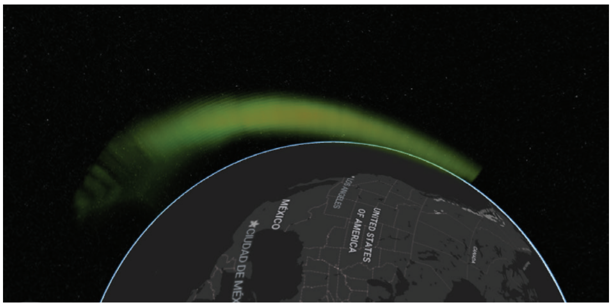

Fig. 44 **– Cesium voxel rendering with ray marching for simulated DMSP fragmentation cloud, December 2024.**

The cloud was visualized as shown in Appendix 2, with **Fig.** ***54*** being the non-interactive rendering and then **Fig.** ***55*** sporting a clean slider bar interface to allow the user to interact with the data.

This volumetric display test was successful, so COMSPOC and Cesium will now explore its direct application within Spacebook.

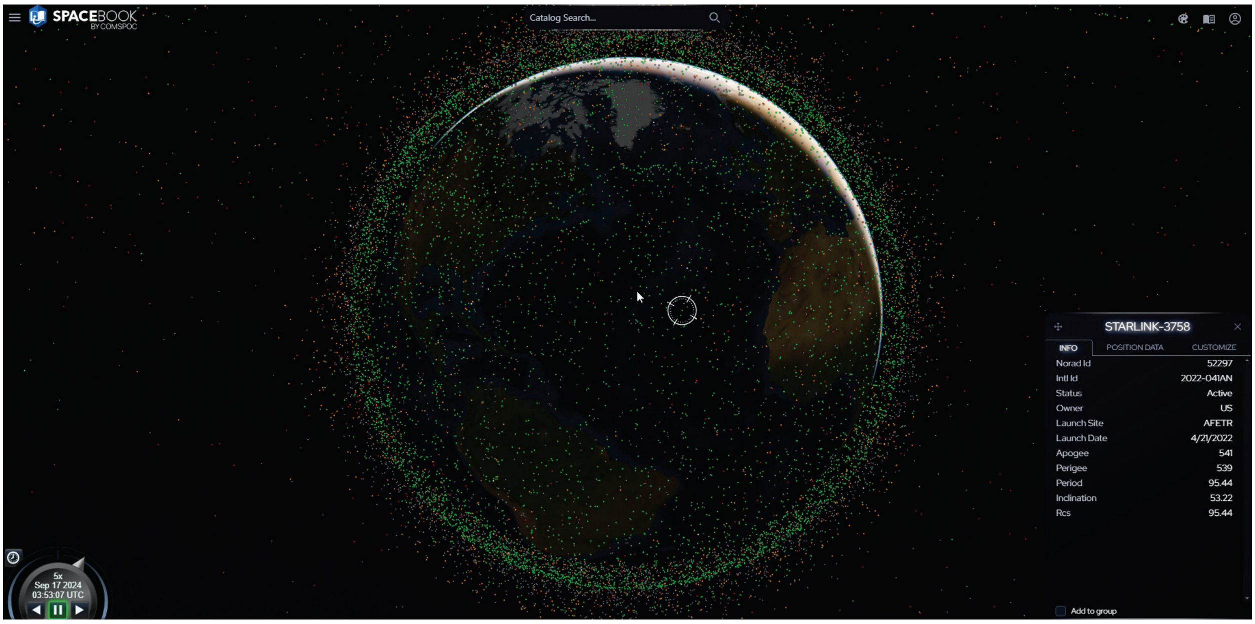

Fig. 45 – ***Spacebook Explorer with Object Window for Starlink-3758 at lower right.***

Fig. 46 – ***Searching the catalog for all spacecraft owned by Brazil launched after 1 January 2010.***

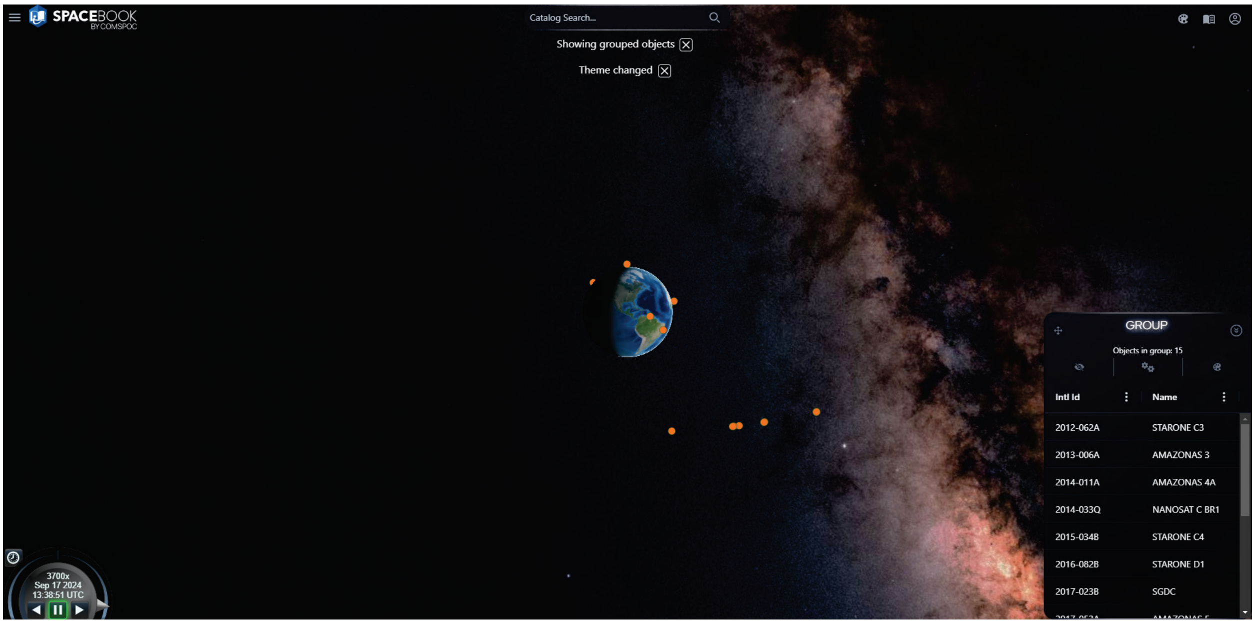

Fig. 47 – ***Explorer showing only objects in the defined group.***

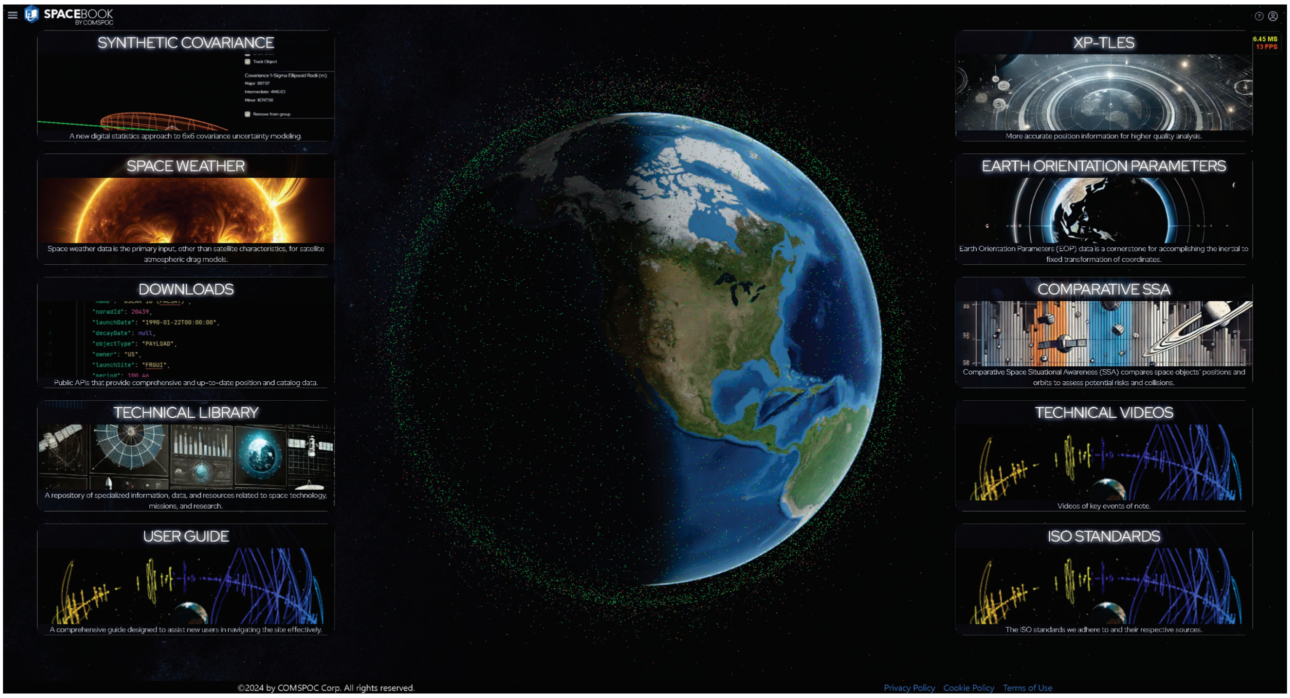

Fig. 48 – ***User interface for downloading Spacebook products.***

13 Training and education

13.1 CSSI Technical Library

The technical library card links to COMSPOC's website, to a page that contains research done by COMSPOC dating back to 2002. The page lists the title of the paper or presentation, which event or publication it is associated with, and a link to download the content. Research on a specific topic can be found using the library's search feature.

13.2 Technical videos

The technical videos card links to COMSPOC's website, to a page that contains videos produced by COMSPOC's research and operations teams. These videos show recent space events that have happened in space, as well as modelling and predictions of potential threats and the results of numerous space safety, sustainability, Space

Traffic Coordination (STC) and Management (STM), and astrodynamics research studies, to name a few.

13.3 Space standards

Spacebook includes guiding information on the various space standards developed in ISO and CCSDS, as well as industry best practices documents and initiatives. This area will gradually be populated throughout 2025.

14 Conclusion

This paper provides a brief overview of the new Spacebook portal. Spacebook will continue to evolve to best serve the needs of the space community, and we welcome your feedback, questions, and suggested enhancements to make Spacebook the portal of choice for flight safety, SSA, and SDA operations.

15 Acknowledgements

We are grateful to all participants and contributors that made Spacebook possible, including the U.S. government, commercial spacecraft operators, commercial SSA service providers, the Space Data Association for their support, Jonathan McDowell, the Secure World Foundation, the University of Texas, and the Center for Strategic and International Studies.

Appendix 1. Characterizations of principle error ellipsoid frame sigma values for sample synthetic covariances

The following figures provide graphical characterizations of a variety of synthetic covariances on a logarithmic precision scale (y-axis). In each plot, the title indicates what the source of the reference orbit was, while the logarithmic scale allows all data to be clearly shown on a single plot (the estimated accuracy of the reference orbit is of particular interest), the log scale tends to deemphasize large positional errors while exacerbating small ones.

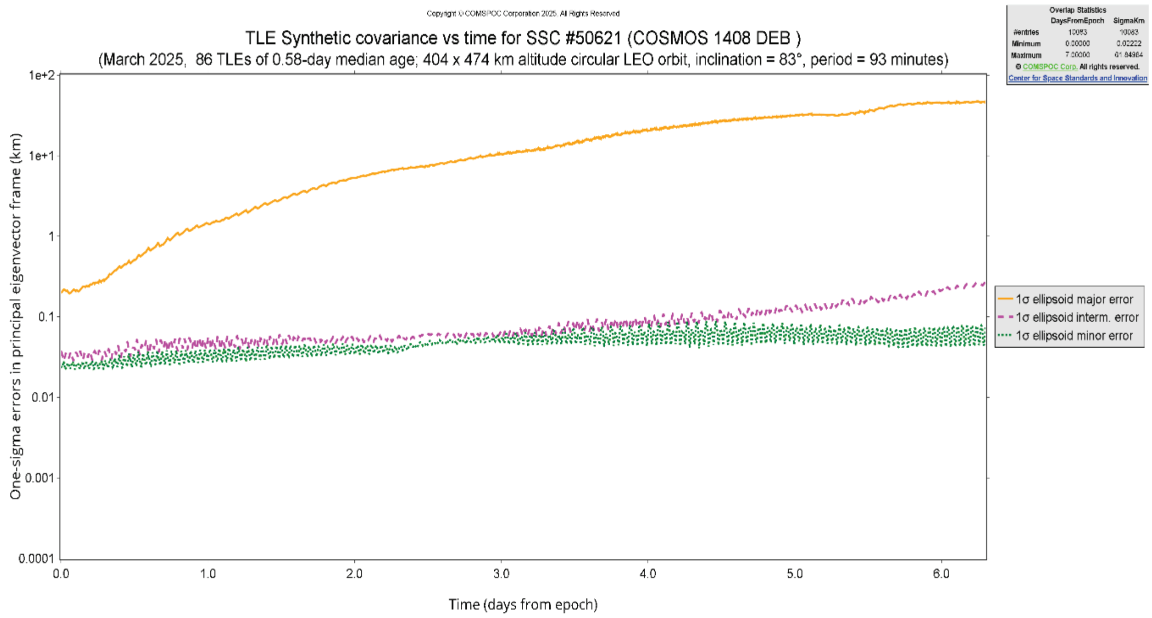

Fig. 49 – *TLE-based synthetic covariance for a COSMOS 1408 debris fragment in LEO.*
Note the slight argument of latitude dependency (≈15.5 revs per day).

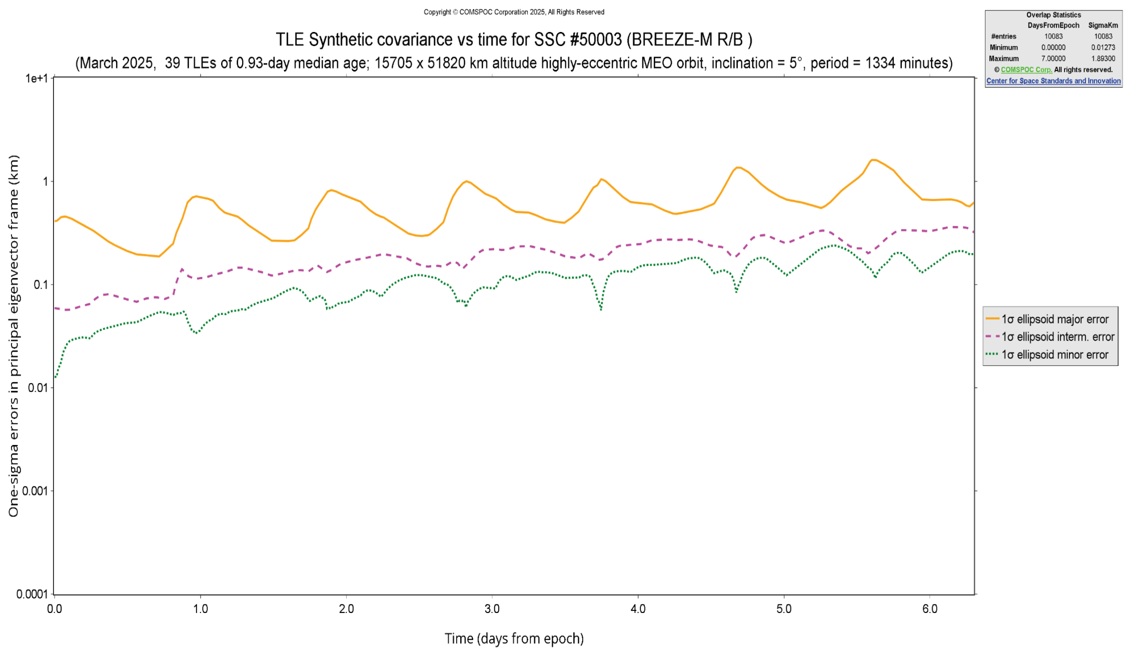

Fig. 50 – *TLE-based synthetic covariance for a derelict Breeze-M rocket body in near-GEO.*
Note the strong argument of latitude dependency (≈ 1 rev per day).

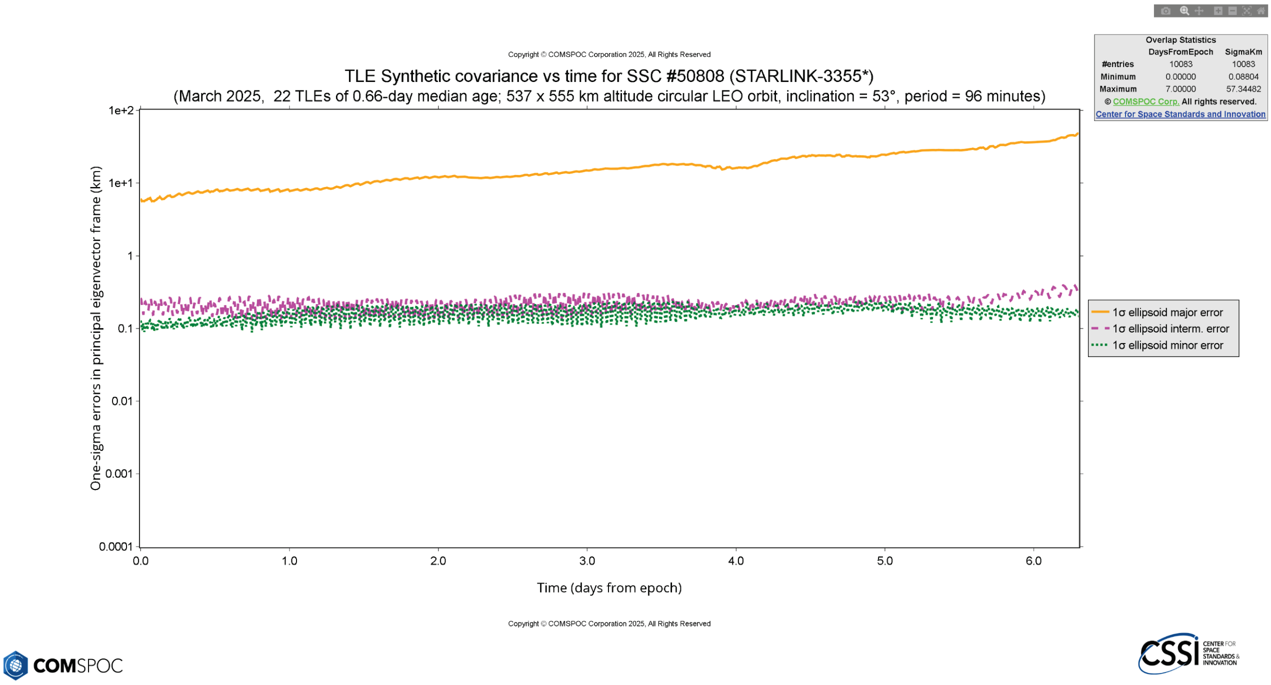

Fig. 51 – *TLE-based synthetic covariance for a Starlink 3355 (active LEO spacecraft).*
Note the poor precision for this maneuvering satellite.

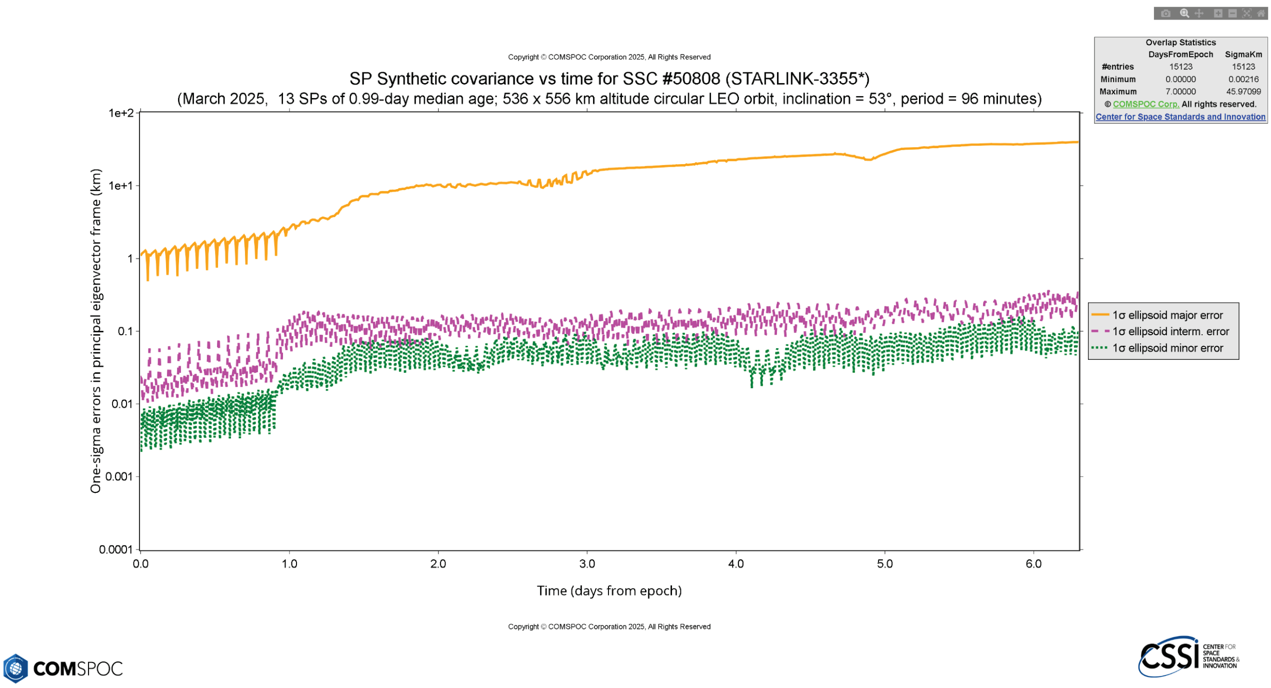

Fig. 52 – *SP-based synthetic covariance for a Starlink 3355 (active LEO spacecraft).*
Note that while SP initially offers improved precision, it matches the TLE's precision after several days.

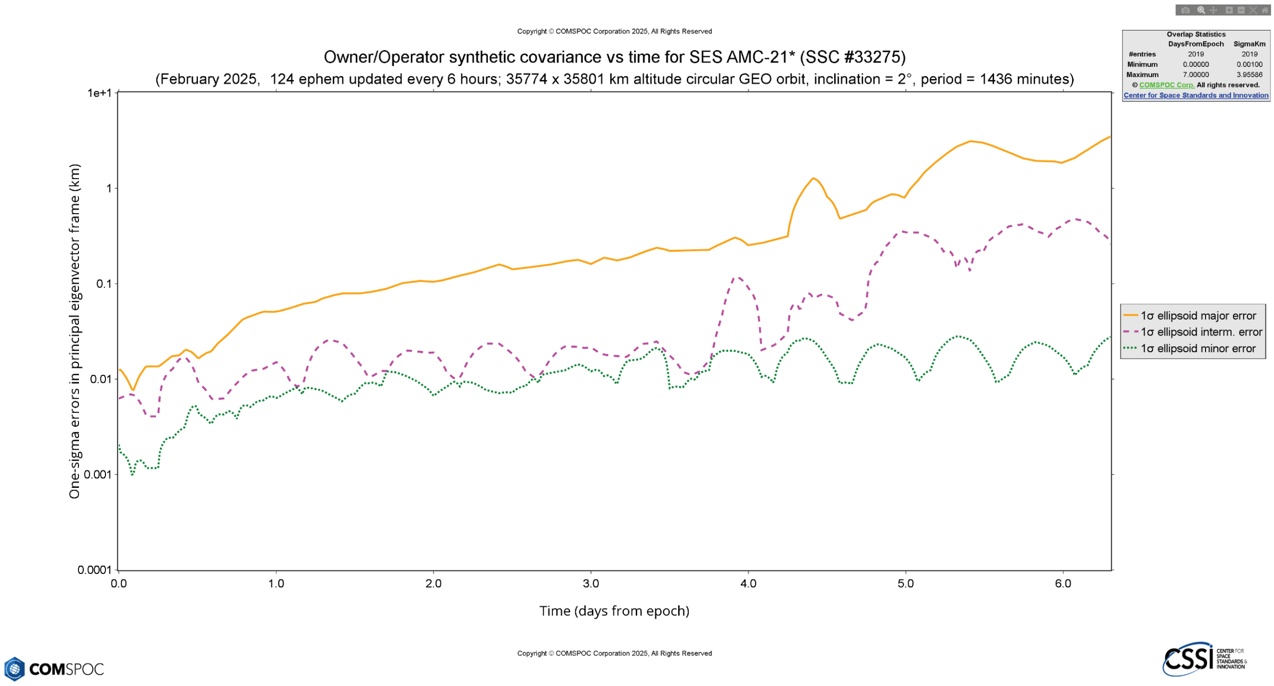

Fig. 53 – *Owner/Operator-based synthetic covariance for a GEO spacecraft (SES AMC-21, uploaded every 2 hours).*

Note how, for this positionally well-maintained spacecraft, has a demonstrably very tight precision of 10 meters is demonstrated at epoch, growing to only several kilometres after one week.

Appendix 2. Volumetric displays of breakup clouds in CesiumJS

This appendix contains several examples and screenshots of the volumetric display that COMSPOC and Cesium partnered to simulate, render, and visualize.

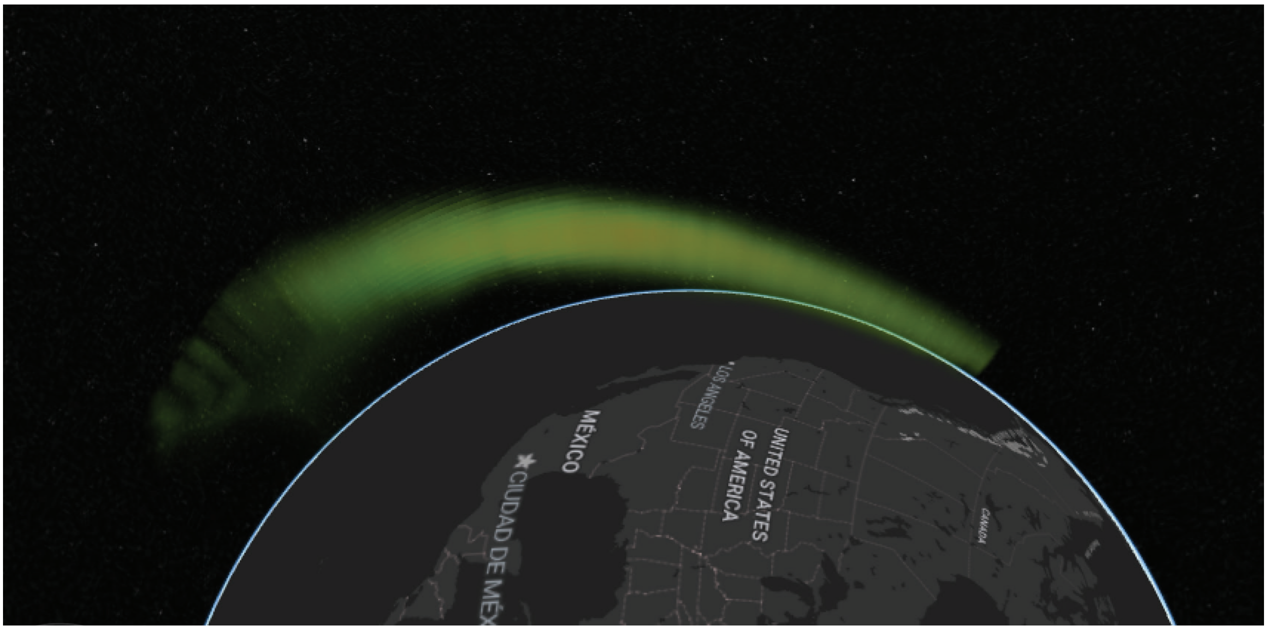

Fig. 54 – ***Volumetric display of simulated DMSP mid-December 2024 breakup, rendered in Cesium.***

Fig. 55 – ***Interactive volumetric display of simulated DMSP mid-December 2024 breakup with slider bars.***

16 References

[1] Vallado, D.A., Alfano, S., Oltrogge, D.L., and Zimmer, P., "Actionability and Persistence of Conjunction Data," Paper #AAS 23-114, AAS/AIAA Astrodynamics Specialist Conference, Big Sky, MT USA, 20 Aug 2023.

[2] Fundamentals of Astrodynamics and Applications, 5th Edition, ISBN 978-1-881883-22-7, David A. Vallado, Published by Microcosm Press, 2022.

[3] Vallado, David A. and T.S. Kelso. 2015. New Consolidated Files for Earth Orientation Parameters and Space Weather Data. Paper AAS-15-500 presented at the AAS/AIAA Astrodynamics Specialist Conference, August 9-13. Vail, CO.

[4] Fundamentals of Astrodynamics and Applications, 4th Edition, ISBN 978-1881883180, David A. Vallado and Wayne D. McClain, Published by Microcosm Press, 2013

[5] ESA's Database and Information System Characterising Objects in Space) (https://discosweb.esoc.esa.int/).

[6] Jonathan C. McDowell's General Catalog of Artificial Space Objects) (https://planet4589.org/).

[7] Space-Track website, https://www.space-track.org/.

[8] CelesTrak website, https://celestrak.org/.

[9] Rich, Adam T., "Investigating Analytical and Numerical Methods to Predict Satellite Orbits Using Two-Line Element Sets" (2017). Theses and Dissertations. 1722.

[10] Gist, R.G., Oltrogge, D.L., and Alfano, S., "Synthetic Covariance Production Using a New Digital Approach," IAA-ICSSA-24-16317, 4TH International Conference on Space Situational Awareness (ICSSA), Daytona Beach, FL, USA, 8 May 2024.

[11] Press, William H.; Teukolsky, Saul A.; Vetterling, William T.; Flannery, Brian P. (1992). Numerical recipes in C: the art of scientific computing (2nd ed.). New York, NY, USA: Cambridge University Press. pp. 123-128.

[12] Mason, J., "Development of a MATLAB/STK TLE Accuracy Assessment Tool, in Support of the NASA Ames Space Traffic Management Project", International Space University, Space Studies Thesis, 2009.

[13] T.S. Kelso, T. S., "Validation of SGP4 and IS-GPS-200D Against GPS Precision Ephemerides", Paper AAS 07-127, 17th AAS/AIAA Space Flight Mechanics Conference, January 28–February 1, 2007, Sedona, Arizona.

[14] Oltrogge, D.L., Chan, J., Vallado, D.A., Cornelius, J., D'Uva, A.R., Hall, R.A., "Deep Operator and SSA Collaboration for Space Sustainability", 12th IAASS Conference, Osaka, Japan, 23 May 2023.

[15] Oltrogge, D.L., Wauthier, P., Vallado, D.A., Alfano, S. and Kelso, T.S., "Results of comprehensive STCM data fusion experiment," 11th European Conference on Space Debris, 23 April 2021.

[16] Oltrogge, D.L., Chan, J., Vallado, D.A., Cornelius, J.J., D'Uva, A., and Hall, R.A., "Deep operator and SSA collaboration for space sustainability," Journal of Space Safety Engineering Vol II, Issue 2, June 2024, pp. 342-361, freely downloadable at: https://doi.org/10.1016/j.jsse.2024.03.007 .

[17] DISCOS (Database and Information System Characterising Objects in Space), European Space Agency, https://discosweb.esoc.esa.int/

[18] Alfano, S., Oltrogge, D.L., Krag, H., Merz, K., and Hall, R.H., "Risk assessment of recent high-interest conjunctions," Acta Astronautica 2021, https://doi.org/10.1016/j.actaastro.2021.04.009, 7 April 2021, accessible at https://comspoc.com/Resources/Content/Private/C-20220424T160558/Paper/20210501_Risk_Assessment_of_High_Interest_Conj_Aeolus_Starlink_AA_Gold_Open_Access.pdf.

[19] Yuchen Xie and Ken Chan, "Collision Probability for Rectangular Cross Sections," Paper No. AIAA 2018-2231, 2018 Space Flight Mechanics Meeting, Jan 9-12, 2018, Kissimmee, Florida.